Tailoring ZnSe–CdSe Colloidal Quantum Dots *via* Cation Exchange: From Core/Shell to Alloy Nanocrystals

Esther Groeneveld,[†] Leon Witteman,[†] Merel Lefferts,[†] Xiaoxing Ke,[‡] Sara Bals,[‡] Gustaaf Van Tendeloo,[‡] and Celso de Mello Donega[†,*]

[†]Condensed Matter and Interfaces, Debye Institute for Nanomaterials Science, Utrecht University, 3508 TA Utrecht, The Netherlands and [‡]EMAT, University of Antwerp, Groenenborgerlaan 171, B-2020 Antwerp, Belgium

ABSTRACT We report a study of Zn^{2+} by Cd^{2+} cation exchange (CE) in colloidal ZnSe nanocrystals (NCs). Our results reveal that CE in ZnSe NCs is a thermally activated isotropic process. The CE efficiency (*i.e.*, fraction of Cd^{2+} ions originally in solution, Cd_{sol}, that is incorporated in the ZnSe NC) increases with temperature and depends also on the Cd_{sol}/ZnSe ratio. Interestingly, the reaction temperature can be used as a sensitive parameter to tailor both the composition and the elemental distribution profile of the product (Zn,Cd)Se NCs. At 150 °C ZnSe/CdSe core/shell hetero-NCs (HNCs) are obtained, while higher temperatures (200 and 220 °C) produce $(Zn_{1-x}Cd_x)Se$ gradient alloy NCs, with increasingly smoother gradients as the temperature increases, until homogeneous alloy NCs are obtained at $T \geq 240$ °C. Remarkably, sequential heating (150 °C followed by 220 °C) leads to ZnSe/CdSe core/shell HNCs with thicker shells, rather than $(Zn_{1-x}Cd_x)Se$ gradient alloy NCs. Thermal treatment at 250 °C converts the ZnSe/CdSe core/shell HNCs into $(Zn_{1-x}Cd_x)Se$ homogeneous alloy NCs, while preserving the NC shape. A mechanism for the cation exchange in ZnSe NCs is proposed, in which fast CE takes place at the NC surface, and is followed by relatively slower thermally activated solid-state cation diffusion, which is mediated by Frenkel defects. The findings presented here demonstrate that cation exchange in colloidal ZnSe NCs provides a very sensitive tool to tailor the nature and localization regime of the electron and hole wave functions and the optoelectronic properties of colloidal ZnSe–CdSe NCs.

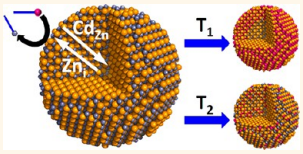

KEYWORDS: cation exchange · ZnSe · ZnSe–CdSe · core–shell nanocrystals · gradient alloy nanocrystals · quantum dots

Colloidal semiconductor nanocrystals (NCs) form a new class of versatile materials that combine size- and shape-dependent properties with easy surface manipulation and solution processing.[1] NCs consisting of two (or more) different semiconductors joined by heterointerfaces (*i.e.*, heteronanocrystals, HNCs) offer even more exciting possibilities regarding property engineering, since the spatial localization of charge carriers in these nanomaterials can be manipulated by controlling the offsets between the energy levels of adjoining segments.[1] This can be achieved by tailoring the composition, size, and shape of each segment, as well as the overall architecture of the HNC.[1] In type-I HNCs the energy offsets are such that both carriers are confined in the same segment, whereas in type-II HNCs the electron and hole wave functions are primarily localized in different segments, leading to the formation of a spatially indirect exciton.[1] Type-I$^{1/2}$ HNCs (also known as quasi-type-II HNCs)[2] form an intermediate localization regime and are characterized by the localization of one charge carrier in one of the segments, while the other carrier is delocalized over the whole volume of the HNC.[1] These tunable properties make HNCs interesting materials for a number of applications (*e.g.*, lasers, solar energy conversion, LEDs, biomedical imaging).

Some semiconductor material combinations (*e.g.*, ZnSe–CdS,[2,3] ZnTe–CdSe,[4] CdTe–CdSe[5]) allow the charge carrier localization regime in core/shell HNCs to be gradually tailored from type-I to type-II by varying the shell thickness and core diameter. ZnSe–CdSe is such a material combination. The band alignment in the bulk limit is type-I (electron and hole in CdSe),[1] but can be tuned from type-I to type-II in CdSe/ZnSe and ZnSe/CdSe concentric core/shell HNCs.[6–9] Thin ZnSe shells over CdSe cores yield type-I HNCs,[6,7] while sufficiently thick shells result in type-II HNCs (hole in the ZnSe shell).[8] Thin CdSe shells over ZnSe cores also yield type-I HNCs (electron and hole in the core), although in

* Address correspondence to C.demello-donega@uu.nl.

Received for review June 10, 2013 and accepted August 13, 2013.

Published online August 13, 2013
10.1021/nn402931y

this case the confinement potential is not sufficiently large to prevent the electron and hole wave functions from reaching the HNC surface.[9] For sufficiently thick CdSe shells an inverted type-I HNC (*i.e.*, electron and hole in the shell) is obtained.[9] Interestingly, CdSe shells of intermediate thickness (~1−1.6 nm, depending on the ZnSe core diameter) yield HNCs in the type-I$^{1/2}$ regime (electron in the CdSe shell, hole delocalized over the HNC).[2,9]

Another attractive feature of the ZnSe−CdSe system is that the two materials are fully miscible, allowing $(Zn_{1-x}Cd_x)Se$ alloy NCs of any arbitrary composition to be readily synthesized, either directly or by thermal annealing of CdSe/ZnSe core/shell HNCs.[10−14] Depending on the synthesis conditions, $(Zn_{1-x}Cd_x)Se$ NCs can be obtained as fully homogeneous solid solutions or as gradient alloys in which the NC composition gradually changes from its center to the surface (*e.g.*, center is Cd-rich, while the surface is Zn-rich). $(Zn_{1-x}Cd_x)Se$ alloy NCs have attracted increasing attention in recent years, due to their high luminescence quantum yields, high stability, and spectral tunability in the blue-yellow region without the need to change the NC size.[10−14] $(Zn_{1-x}Cd_x)Se$ gradient alloy NCs are also gaining importance as nonblinking single luminophores.[14]

The intense research activity in the field of colloidal NC synthesis has resulted in a significant degree of size and shape control over NCs and HNCs[1,15−17] and has yielded various HNC morphologies, such as concentric core/(multi)shell HNCs, heterodumbbells, and heteronanorods. Colloidal HNCs are typically synthesized by heteroepitaxial growth over a pre-existing NC seed. However, heteroepitaxial growth is prevented for some material combinations by large lattice mismatches or thermal instability of the NC seed at the required reaction temperatures.[1] Recently, cation exchange has emerged as a versatile alternative strategy for accessing NC and HNC compositions and morphologies that would not be attainable by conventional methods.[18−27] This approach has led to the successful preparation of complex HNCs, such as PbSe/CdSe core/shell HNCs (dots, cubes, rods),[20−22] PbSe/PbS dot core/rod shell heteronanorods,[23] CdS/CuS heterorods,[24] and CdSe/CdS hetero-octapods.[25] Cation exchange has also been used to introduce dopants in NCs (*e.g.*, ZnTe:Mn,[28] InAs:Cu, Ag or Au,[29] and CdSe:Ag).[30]

Nanoscale cation exchange reactions have been extensively investigated for aliovalent systems (M^{2+} for M^{+} cations, *e.g.*, Cd^{2+} for Ag^{+} or Cu^{+}).[18,19,23−26] Isovalent cation exchange studies have received much less attention and have been mostly restricted to Pb^{2+} for Cd^{2+} in PbX NCs (X = S, Se, Te).[20−22] Since PbX and CdX are immiscible and present very small lattice mismatches, these exchange reactions yield either core/shell HNCs or fully exchanged CdX NCs.[20−22] Despite the importance of ZnX-based NCs and HNCs, studies addressing the direct exchange of Zn^{2+} by other M^{2+} cations are scarce and have appeared only very recently (*viz.*, Zn^{2+} for Cd^{2+} and Zn^{2+} for Mn^{2+} in ~2 nm diameter ZnTe magic size clusters,[28,31] and Zn^{2+} for Cd^{2+} in 3 nm diameter ZnSe NCs[32]). The Zn^{2+} for Cd^{2+} place exchange reaction in ZnSe NCs is of particular interest, since it may offer a versatile and efficient approach to tune the charge carrier localization regime in (Zn,Cd)Se NCs while preserving their size and shape. Although previous work has demonstrated only the formation of $(Zn_{1-x}Cd_x)Se$ homogeneous alloy NCs by Zn^{2+} for Cd^{2+} exchange in ZnSe NCs,[32] the possibility that other compositional distribution profiles are attainable as well cannot be excluded, since cation exchange reactions are often under kinetic control, therefore allowing access to metastable structures and kinetically trapped states.[18,19,22,25]

The goal of the present work was to investigate whether the Zn^{2+} for Cd^{2+} exchange reaction in colloidal ZnSe NCs could be used to control the compositional distribution profile of (Zn,Cd)Se NCs, thereby tailoring the charge carrier localization regime and the optoelectronic properties of the resulting nanostructures. Our findings reveal that the reaction temperature can be used as a sensitive parameter to control the elemental distribution profile after the Zn^{2+} for Cd^{2+} exchange reaction, allowing the NCs to be tailored from concentric ZnSe/CdSe core/shell HNCs to $(Zn_{1-x}Cd_x)Se$ homogeneous alloy NCs, through gradient alloy NCs.

RESULTS AND DISCUSSION

Parent ZnSe Nanocrystals. Two different sizes of organically capped colloidal ZnSe NCs were used for the Zn^{2+} for Cd^{2+} exchange reaction: 3.7 ± 0.4 nm diameter and 5.6 ± 0.6 nm diameter. The NCs are nearly spherical and faceted. The X-ray diffraction pattern of the 5.6 nm diameter ZnSe NCs (Figure 1) indicates that the NCs have the zinc blende crystal structure. The absorption spectra (Figures 1A and 2A) consist of multiple features, which are shifted to higher energies with respect to the electronic transitions of bulk ZnSe (E_g= 2.63 eV), as expected since both NC sizes are smaller than the exciton Bohr radius of ZnSe (*viz.*, 3.8 nm). Four different exciton transitions can be distinguished, the lowest energy one being observed at 385 nm (3.22 eV) for the 3.7 nm diameter NCs and at 423 nm (2.93 eV) for the 5.6 nm diameter NCs. Following previous work on CdSe NCs,[33] these exciton transitions can be assigned to $1S_{3/2(h)}-1S_{(e)}$, $2S_{3/2(h)}-1S_{(e)}$, $1S_{1/2(h)}-1S_{(e)}$, and $1P_{3/2(h)}-1P_{(e)}$, from lowest to highest energies, respectively. The full-width at half-maximum (fwhm) of the photoluminescence (PL) peak is 108 meV for the 5.6 nm diameter ZnSe NCs (Figure 1).

Cation Exchange in 3.7 nm Diameter ZnSe NCs. Figure 2A shows the absorption spectra of a series of samples collected at different time points during a Zn^{2+} for

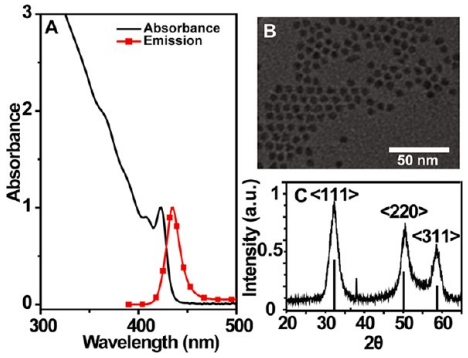

Figure 1. Characteristics of the 5.6 ± 0.6 nm diameter ZnSe parent NCs. (A) Absorption and emission spectra (excitation at 380 nm). (B) Representative TEM image. (C) X-ray diffraction pattern (bars indicate position and relative intensity of diffraction peaks for bulk zinc blende ZnSe).

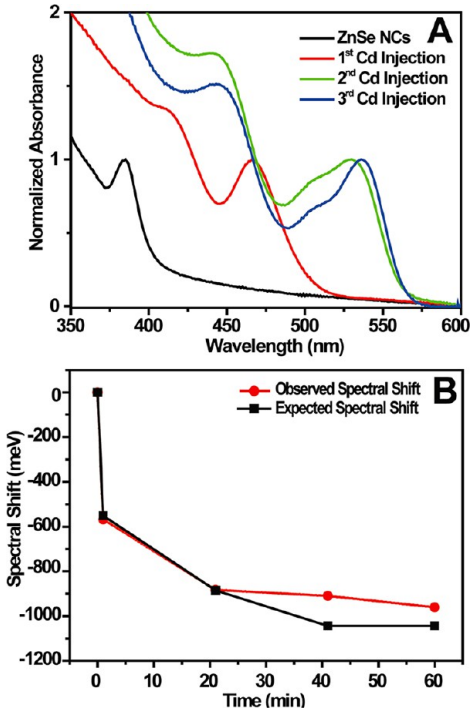

Figure 2. (A) Absorption spectra of a series of samples collected during a Zn^{2+} for Cd^{2+} exchange reaction in 3.7 nm diameter ZnSe NCs at 240 °C. The spectrum of the parent ZnSe NCs is also given. The cation exchange was driven by three sequential injections of Cd-oleate at 0, 20, and 40 min (samples collected 1 min after each addition). (B) Temporal evolution of the spectral shift observed for the lowest energy absorption transition. The expected spectral shift assuming quantitative exchange and formation of $(Zn_{1-x}Cd_x)Se$ homogeneous alloy NCs (see eq 1) is also presented.

Cd^{2+} exchange reaction in 3.7 nm ZnSe NCs at 240 °C. The absorption spectrum of the parent NCs is also presented. The cation exchange was driven by three sequential injections of Cd-oleate at times 0, 20, and 40 min (samples collected 1 min after each addition; see Experimental Methods for details). The absorption transitions shift to lower energies following each Cd addition, clearly demonstrating the formation of $(Zn_{1-x}Cd_x)Se$ NCs as a result of the Zn^{2+} for Cd^{2+} exchange reaction. The temporal evolution of the spectral shift observed for the lowest energy absorption transition is presented in Figure 2B, which also shows the expected spectral shift assuming that the exchange is quantitative and that $(Zn_{1-x}Cd_x)Se$ homogeneous alloy NCs are formed. These assumptions are based on previous work by Zhong *et al.*,[32] who investigated the Zn^{2+} for Cd^{2+} exchange reaction at 220 °C in similarly sized ZnSe NCs (d = 3.1 nm) after single injections of Cd-oleate.

The band gap of bulk $(Zn_{1-x}Cd_x)Se$ solid solutions (*i.e.*, homogeneous alloys) is known to decrease nonlinearly from 2.63 eV (bulk ZnSe band gap, x = 0) to 1.74 eV (bulk CdSe band gap, x = 1) as follows:[34]

$$E_g(Zn_{1-x}Cd_x)Se = 2.63 - [(2.63 - 1.74) + 0.75]x + 0.75x^2 \quad (1)$$

This expression has been shown to be valid also for $(Zn_{1-x}Cd_x)Se$ homogeneous alloy NCs, provided the bulk band gap values are replaced by the corresponding values for ZnSe and CdSe NCs of diameter equal to that of the alloy NCs.[10,12] Equation 1 can thus be used to estimate the expected band gap for the $(Zn_{1-x}Cd_x)Se$ NCs obtained after the Zn^{2+} for Cd^{2+} exchange reaction, assuming that a homogeneous alloy is formed and that all the Cd^{2+} added in solution is exchanged for Zn^{2+} and is thus incorporated in the NC. For the estimates shown in Figure 2B the band gaps of 3.7 nm ZnSe and CdSe NCs were taken to be 3.22 eV (Figure 2A) and 2.16 eV,[35] respectively.

The agreement between expected and observed shifts is excellent up to the second Cd addition, showing that both assumptions are valid up to 70% Zn for Cd replacement (x = 0.7). The results also show that the cation exchange is fast, reaching completion in less than 1 min. After the third addition, when the ratio between the added Cd precursor and the number of ZnSe units reaches 1, the observed shift becomes smaller than expected, even if the reaction is allowed to progress for an additional 20 min (the x value at the end of the reaction is estimated to be 0.8, based on the observed band gap). This implies that the Zn^{2+} for Cd^{2+} exchange rates have slowed down and that the exchange is no longer quantitative, so that larger Cd excesses would be needed to drive the reaction further. We note that this observation is consistent with previously reported results,[32] since complete conversion of ZnSe NCs into CdSe NCs was not observed, even with Cd_{added}/ZnSe ratios equal to 2 (observed x was then 0.96). The larger exchange efficiency reported in ref 32 for a Cd_{added}/ZnSe ratio equal to 1 (*viz.*, 0.94) may be due to the fact that the total amount of Cd was added in a single injection,[32] while in the present work it was divided into three sequential additions. As will be discussed below, the initial Cd concentration has indeed a large impact on the cation exchange kinetics and the exchange efficiency.

Cation Exchange in 5.6 nm Diameter ZnSe NCs: Kinetics and Temperature Dependence. The observations described above suggest that the Zn^{2+} for Cd^{2+} exchange rates may be amenable to control, allowing one to tune the extent of the exchange and the elemental distribution profiles. Larger ZnSe NCs are better suited to investigate the relation between the reaction conditions and the characteristics of the product $(Zn_{1-x}Cd_x)Se$ NCs, since they allow for a more precise determination of size, composition, and elemental distribution profiles. For this reason, the remainder of this work will deal with investigations carried out on 5.6 nm diameter ZnSe NCs.

The absorption and PL spectra of a series of $(Zn_{1-x}Cd_x)Se$ NC samples collected at different time points during a Zn^{2+} for Cd^{2+} exchange reaction in 5.6 nm ZnSe NCs are shown in Figure 3. The spectra of the parent ZnSe NCs are also presented. The reaction was carried out at 220 °C and was driven by a single injection of Cd-oleate (Cd_{added}/ZnSe = 0.23). Figure 3C presents the temporal evolution of the spectral shift of the lowest energy absorption peak for two different reaction temperatures (150 and 220 °C). The reaction conditions were identical, apart from the temperatures. It is clear that the injection of Cd-oleate leads to a fast exchange reaction at both temperatures. Interestingly, a steady state is reached at both temperatures, but the degree of exchange, as judged by the extent of the spectral shift, is smaller at 150 °C, despite identical concentrations of Cd-oleate and Cd_{added}/ZnSe ratios in both cases. Moreover, it takes longer for the exchange reaction to reach the steady state at lower temperatures (40 min at 220 °C and 100 min at 150 °C, Figure 3C).

The exchange reaction quickly resumes upon addition of more Cd-oleate (at 220 °C an additional shift of −300 meV is observed in the course of 20 min, SI, Figure S1). In contrast, adding Zn-oleate in concentrations as large as 20 times that of the Cd-oleate added in the first injection does not lead to any observable blue shift, even after 50 min at 220 °C. This clearly shows that the Zn^{2+} for Cd^{2+} exchange in ZnSe NCs is not reversible under the conditions used in our experiments. This is consistent with observations reported by a number of other groups and with the fact that CdSe/ZnSe core/shell HNCs are routinely grown by the SILAR technique, which involves single injections of Zn precursors into solutions containing CdSe NCs.[6,7,26,32]

It is noteworthy that the PL quantum yields (QYs) of the $(Zn_{1-x}Cd_x)Se$ NCs produced at 220 °C decrease dramatically (*viz.*, from 6% to ∼1%, SI, Figure S2) immediately after the Cd-oleate addition and gradually recover as the steady state is approached, stabilizing at ∼14% for as long as the steady state is maintained (at least up to 190 min). Interestingly, the burst of cation exchange induced by the second Cd injection also leads to a drop in the PL QYs (6%), followed by a pronounced and fast increase to 60% (SI, Figure S2). This behavior is reminiscent of that previously reported for organically capped colloidal CdSe NCs during their growth following the injection of Cd and Se precursors into a hot coordinating solvent.[36] The initial PL QYs of the CdSe NCs were very low (few %) and gradually increased as the growth rates decreased, reaching a maximum (50−80%) only when the NC growth had stopped.[36] Addition of more Cd and Se precursors was reported to lead to a quick burst of NC growth accompanied by a drop in PL QY to a few percent, followed by recovery to values as high as 60%.[36] These observations were interpreted as indicating that the rapid NC growth phase resulted in surface defects and surface

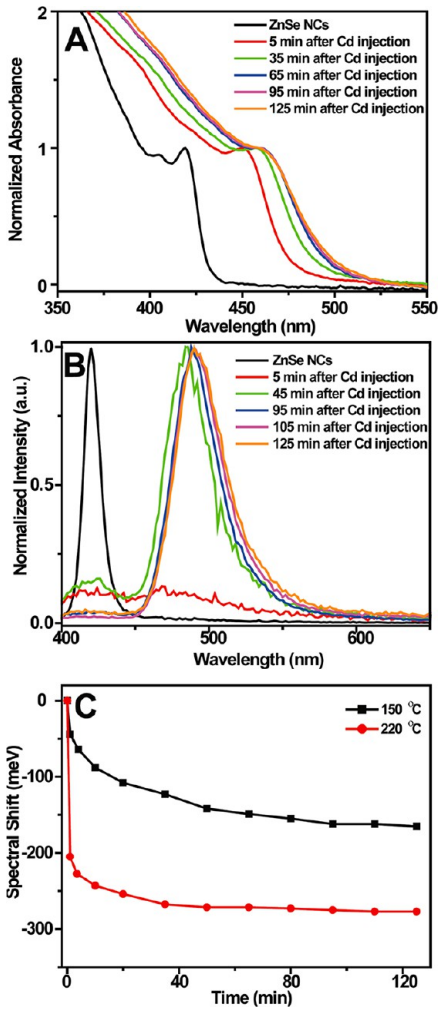

Figure 3. Absorption (A) and PL (B) spectra of a series of samples collected at different time points during a Zn^{2+} for Cd^{2+} exchange reaction in 5.6 nm ZnSe NCs at 220 °C. The spectra of the parent ZnSe NCs are also given. The cation exchange was driven by a single Cd-oleate injection at $t = 0$ (Cd_{added}/ZnSe = 0.23). (C) Temporal evolution of the spectral shift observed for the lowest energy absorption transition of product (Zn,Cd)Se NCs obtained by cation exchange in 5.6 nm ZnSe NCs at two different temperatures (150 and 220 °C) (all other reaction parameters were identical). The temporal evolution of the PL quantum yields for the same series of samples is presented in the SI (Figure S2).

disorder, which were removed by surface relaxation and/or reconstruction during the annealing phase under near-zero growth rates.[36] The present observations (SI, Figure S2a,b) can thus be rationalized as indicating that defects (and/or disorder) are created in the $(Zn_{1-x}Cd_x)Se$ NCs at early stages of the cation exchange reaction and are subsequently eliminated by annealing during the steady state. The fact that the PL QYs of the product $(Zn_{1-x}Cd_x)Se$ NCs do not recover when the cation exchange reaction is performed at 150 °C (SI, Figure S2c,d) shows that the annealing of the defects created during the fast exchange phase can take place only at sufficiently high temperatures.

To investigate the impact of the temperature in more detail, Zn^{2+} for Cd^{2+} cation exchange reactions were carried out at four different temperatures (150, 200, 220, and 250 °C), for the same period of time and using identical conditions (see Experimental Methods for details). The upper limit for the reaction temperature (250 °C) was set based on control experiments (SI, Figure S3), which established that ripening of the ZnSe NCs quickly occurred at $T \geq 270$ °C, under the conditions used in the cation exchange reactions. A reaction using sequential heating at two different temperatures was also investigated. In this case, the cation exchange was first carried out at 150 °C for the same period of time used for the other samples (80 min), and subsequently the temperature was raised to 220 °C over 20 min and kept constant for 5 min before terminating the reaction. To allow a larger degree of exchange to be achieved, three sequential injections of Cd-oleate were used (at t = 0, 20, and 40 min). A single injection containing the same amount of Cd-oleate was observed to lead to larger spectral shifts (*viz.*, −740 meV instead of −530 meV, at 220 °C), accompanied by an increase in size polydispersity and reshaping from nearly spherical to prolate NCs (SI, Figure S4). As will be discussed below, this internal ripening is probably a result of very fast cation exchange rates, which induce a rapid increase in lattice strain within the product (Zn,Cd)Se NCs.

A control experiment was also carried out to evaluate the potential impact on the cation exchange reaction of the excess of oleic acid present in the Cd-oleate solution (SI, Figure S5). Although the concentration of free oleic acid introduced in the reaction medium with the Cd-oleate solution is comparable to that present in the growth solution of the parent ZnSe NCs (260 and 200 mM, respectively), oleic acid has been shown to be a ripening agent for CdSe NCs[37] and may thus potentially affect ZnSe NCs as well. Nevertheless, the control experiment summarized in Figure S5 (SI) clearly demonstrates that the cation exchange rates and the size polydispersity of the product $(Zn_{1-x}Cd_x)Se$ NCs are not affected by free oleic acid at the concentrations present in our cation exchange experiments. Interestingly, the excess of oleic acid is actually beneficial, since the $(Zn_{1-x}Cd_x)Se$ NCs produced under 4 mM free oleic acid had very low PL QYs. It is as yet unclear whether the beneficial impact of oleic acid on the PL QYs of the product $(Zn_{1-x}Cd_x)Se$ NCs is due to a better surface passivation or to an adjuvant role in the relaxation and reconstruction of the NC surfaces during the steady state,[1] or to a combination of both.

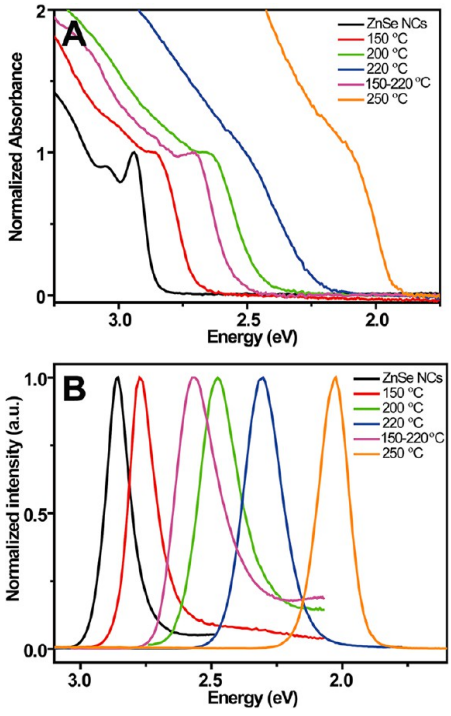

Figure 4. Absorption (A) and PL (B) spectra of (Zn,Cd)Se NCs obtained by Zn^{2+} for Cd^{2+} exchange in 5.6 nm ZnSe NCs at different reaction temperatures (150, 200, 220, 250 °C, samples S150, S200, S220, and S250, respectively). A sample obtained by carrying out the exchange reaction at two consecutive temperatures is also included (80 min at 150 °C, followed by heating to 220 °C in 20 min, and 5 min at 220 °C, sample S150−220). The cation exchange was driven by three sequential injections of Cd-oleate at 0, 20, and 40 min. The total reaction time was 80 min in all cases, except for sample S150−220. All other reaction parameters were identical. The spectra of the parent ZnSe NCs are also shown. The PL quantum yields are 2%, 50% (75% if trap PL is included), 21% (27% if trap PL is included), 80%, and 40%, for samples S150, S150−220, S200, S220, and S250, respectively.

The absorption and PL spectra of the product $(Zn_{1-x}Cd_x)Se$ NCs obtained at different reaction temperatures are shown in Figure 4. Representative TEM images of the product $(Zn_{1-x}Cd_x)Se$ NCs are given in Figure 5. Table 1 collects selected key characteristics of the product $(Zn_{1-x}Cd_x)Se$ NCs. The results summarized in Figure 4 and Table 1 clearly show that the degree of cation exchange increases with the reaction temperature. Therefore, a larger shift of the optical transitions to lower energies is observed for reactions carried out at higher temperatures, despite identical $Cd_{added}/ZnSe$ ratios and initial Cd-oleate concentrations. Nevertheless, the observed spectral shifts are smaller than those

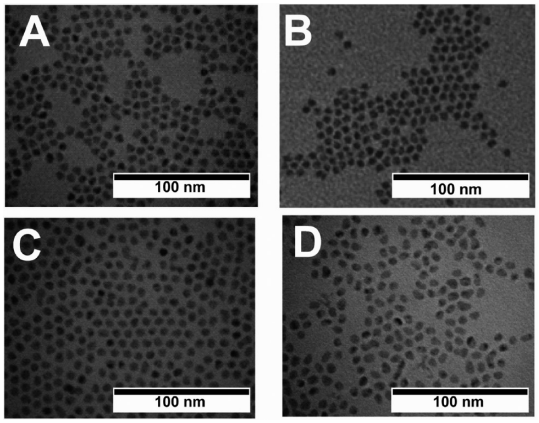

Figure 5. Representative TEM images of (Zn,Cd)Se NCs obtained by Zn^{2+} for Cd^{2+} exchange in 5.6 nm ZnSe NCs at different temperatures: (A) 150 °C (sample S150); (B) two consecutive temperatures: 150 °C, followed by 220 °C (sample S150−220); (C) 220 °C (sample S220); and (D) 250 °C (sample S250). The average NC diameters are given in Table 1. The cation exchange was driven by three sequential injections of Cd-oleate at 0, 20, and 40 min. Total reaction time was 80 min for (A), (C), and (D) and 105 min for (B) (80 min at 150 °C followed by heating to 220 °C over 20 and 5 min at 220 °C). All other reaction parameters were identical.

TABLE 1. Composition and Properties of $(Zn_{1-x}Cd_x)Se$ NCs Obtained by Zn^{2+} for Cd^{2+} Cation Exchange in 5.6 nm Diameter ZnSe NCs at Different Temperatures[a]

sample	T (°C)	x	E_g (eV)	ΔE_{obs} (meV)	$\Delta E_{exp,ha}$ (meV)	d_{obs} (nm)	$d_{exp,ha}$ (nm)
ZnSe		0	2.93	0	0	5.6	
S150	150	0.26	2.85	−83	−389	5.6	5.69
S150−220	150 + 220	0.42	2.64	−290	−580	5.6	5.75
S220	220	0.44	2.40	−530	−600	5.8	5.76
S250	250	0.64	2.13	−800	−790	6	5.83

[a] The parent ZnSe NCs are also included. x = determined from elemental concentrations measured by STEM-EDS (see SI, Table S1 for details). E_g = observed band gap value, determined from the lowest energy absorption peak (Figure 4). ΔE_{obs} = difference between observed E_g and that of the parent ZnSe NCs. $\Delta E_{exp,ha}$ = difference between expected E_g and that of the parent ZnSe NCs. The expected E_g values are calculated using eq 1, which implies the assumption that the product NCs are $(Zn_{1-x}Cd_x)Se$ homogeneous alloy NCs. The band gap of 5.6 nm ZnSe NCs is 2.93 eV (Figure 1A). The band gaps of CdSe NCs are taken to be 1.99, 1.98, 1.975, and 1.97 eV, from S150 to S250, respectively.[35] A graphical comparison between ΔE_{obs} and $\Delta E_{exp,ha}$ is presented in the SI (Figure S6). d_{obs} = observed NC diameter (Figure 1 for parent ZnSe NCs, Figure 5 for product $Zn_{1-x}Cd_xSe$ NCs). The size polydispersity is 10% for all samples, except S250. This sample consists of prolate NCs with aspect ratio ∼1.5 (Figure 5D), and the longest dimension is given as the diameter (±15%). $d_{exp,ha}$ = expected diameter assuming that the product NCs are $(Zn_{1-x}Cd_x)Se$ homogeneous alloy NCs and that the lattice is fully relaxed, *i.e.*, the unit cell has expanded as a function of x following Vegard's law (expected volume expansion = 5%, 8.4%, 8.8%, 12.8%, from x = 0.26 to 0.64, respectively).

expected assuming that the product $(Zn_{1-x}Cd_x)Se$ NCs consist of homogeneous alloys, except for S250 (Table 1 and Figure S6, SI). This is quite remarkable and implies that the elemental distribution profiles deviate from homogeneous solid solutions for all $(Zn_{1-x}Cd_x)Se$ NCs samples prepared at temperatures below ∼250 °C. The deviation increases with decreasing reaction temperatures and is also sensitive to the thermal history of the sample (Table 1 and Figure S6, SI). This is most obvious in the dramatic difference between the optical properties of S220 and S150−220, despite their similar sizes and compositions (Figures 4 and 5, Table 1, and Figure S6). These observations imply that in order to fully understand the impact of the reaction temperature on the Zn^{2+} for Cd^{2+} exchange kinetics and on the optical properties of the product $(Zn_{1-x}Cd_x)Se$ NCs, the elemental distribution profiles of the NCs must be known. This issue will be addressed in detail later, after the analysis of the impact of the temperature on the size and shape of the product $(Zn_{1-x}Cd_x)Se$ NCs.

The size and shape of the product $(Zn_{1-x}Cd_x)Se$ NCs (Figure 5) are essentially the same as those of the parent ZnSe NCs, except for S250, which consists of prolate NCs (aspect ratio ∼1.5) (Figure 5D). Moreover, the elemental analysis of the product $(Zn_{1-x}Cd_x)Se$ NCs shows that the (Cd+Zn)/Se ratio is basically the same, regardless of the reaction temperature (SI, Table S1). It should be noted that Cd^{2+} is larger than Zn^{2+} (*viz.*, 0.78 Å *versus* 0.60 Å, respectively, for tetrahedral sites), which results in larger lattice parameters for CdSe than for ZnSe (*viz.*, 6.05 and 5.668 Å, respectively, for the zinc blende structure). Since $(Zn_{1-x}Cd_x)Se$ solid solutions obey Vegard's law, the lattice parameters of homogeneous alloys increase linearly with the Cd content. Considering that the total number of MSe units in the parent ZnSe NCs is preserved in the product NCs, the volume of the $(Zn_{1-x}Cd_x)Se$ NCs should increase as the Zn^{2+} for Cd^{2+} exchange progresses, if a homogeneous alloy is formed.

The expected diameters for the product $(Zn_{1-x}Cd_x)Se$ NCs, assuming the formation of fully relaxed homogeneous alloy NCs, are listed in Table 1. The lattice expansion induced by the Zn^{2+} for Cd^{2+} exchange in ZnSe NCs can explain the shape distortion observed in the product $(Zn_{1-x}Cd_x)Se$ NCs obtained at 250 °C (Figure 5D). The relatively plastic nature of the ZnSe NCs at this temperature and the abrupt rise in internal NC strain due to the rapid exchange of a substantial amount of Zn^{2+} could lead to uneven expansion of the NC and also facilitate intra-NC ripening. The shape distortion observed upon addition of the total amount of Cd-oleate in a single injection instead of three sequential injections (SI, Figure S4) has probably the same origin. Interestingly, if sample S150−220 is further heated to 250 °C, the shape of the NCs is preserved (SI, Figure S7). This shows that the thermally induced ripening is prevented by the presence of CdSe in the NCs. As will be discussed below, this is also related to the composition profile of sample S150−220 (core/shell HNC). The observed diameters for samples S150 and S150−220 appear to be smaller than expected for fully relaxed $(Zn_{1-x}Cd_x)Se$ homogeneous alloy NCs (Table 1),

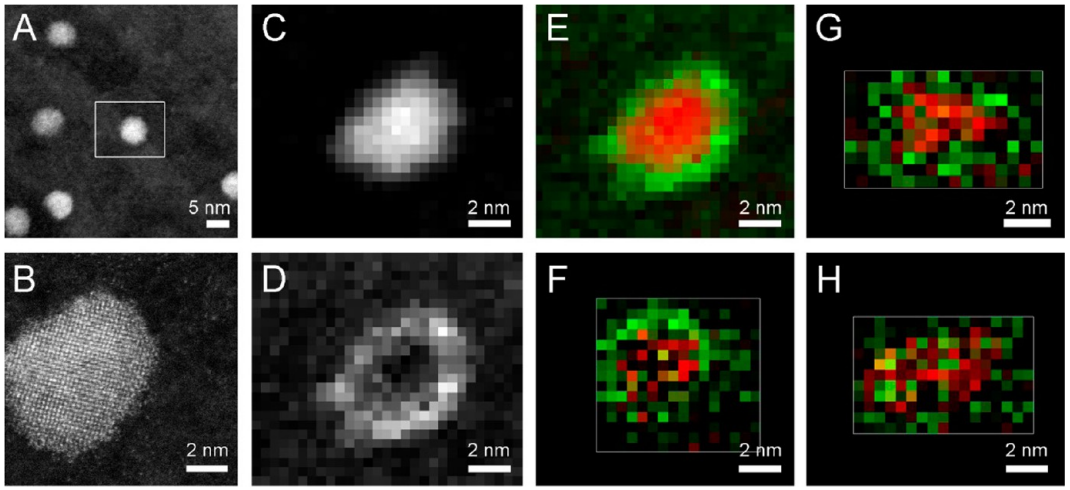

Figure 6. (A) STEM-HAADF images of (Cd,Zn)Se NCs obtained from 5.6 nm ZnSe NCs by Zn^{2+} for Cd^{2+} exchange at two consecutive temperatures (80 min at 150 °C, followed by heating to 220 °C in 20 min, and 5 min at 220 °C) (sample S150−220). The square indicates the region selected for EELS analysis. (B) HR-STEM image of a representative (Cd,Zn)Se NC from sample S150−220 (additional HR-STEM images and an analysis of the structure of the NCs are presented in the SI, Figure S8). Chemical maps for Zn (C) and Cd (D) of the (Cd,Zn)Se NC selected in (A). These maps are combined in (E) to produce a chemical distribution profile of the NC (Zn in red, Cd in green). Chemical distribution profile maps for the product (Cd,Zn)Se NCs obtained by carrying out the Zn^{2+} for Cd^{2+} cation exchange reaction at 220 °C (sample S220) or 200 °C (sample S200) are shown in panels (F) and (G), respectively. The reaction parameters for samples shown in (A)−(G) were identical, except for the temperatures. Panel (H) gives the chemical distribution profile map for a sample obtained by heating the ZnSe/CdSe core/shell HNCs shown in (A)−(E) (sample S150−220) at 250 °C for 20 min (sample S150−220−250). Additional STEM-HAADF images and EELS data for samples S150, S200, S220, and S150−220−250 are provided in the SI (Figures S9−S12).

implying that these samples have rather different elemental composition profiles, in agreement with the conclusions derived from the optical properties of these samples. These points will be addressed in more detail in the next two sections.

Cation Exchange in 5.6 nm Diameter ZnSe NCs: Elemental Distribution Profiles of the Product $(Zn_{1-x}Cd_x)Se$ NCs. The elemental distribution profiles of the product $(Zn_{1-x}Cd_x)Se$ NCs obtained at different reaction temperatures were investigated by high-angle annular dark-field (HAADF) high-resolution scanning transmission electron microscopy (HR-STEM) and STEM-electron energy loss spectroscopy (EELS). Figure 6 shows a representative HR-STEM image, EELS elemental maps for Cd and Zn, and a combined Cd−Zn elemental map for sample S150−220. Combined Cd−Zn elemental maps for samples S200, S220, and S150−220−250 are also shown in Figure 6. The Cd concentration in sample S150 was too low to yield reliable EELS elemental maps. Representative STEM images and EELS elemental maps for samples S150, S200, S220, and S150−220−250 are given in the SI (Figures S8 to S12).

The EELS elemental maps (Figure 6) clearly show that the $(Zn_{0.58}Cd_{0.42})Se$ NCs obtained by carrying out the Zn^{2+} for Cd^{2+} exchange at 150 °C for 80 min and subsequently briefly heating the reaction mixture at 220 °C (sample S150−220) consist of ZnSe/CdSe core/shell HNCs. Since sample S150−220 was obtained from S150, one can conclude that the $(Zn_{0.74}Cd_{0.26})Se$ NCs obtained at 150 °C also consist of ZnSe/CdSe core/shell HNCs, albeit with thinner shells. The shell thickness and core diameter of both ZnSe/CdSe HNC samples can be estimated from their compositions and total diameter (Table 1). This analysis indicates that the $(Zn_{0.74}Cd_{0.26})Se$ HNCs (sample S150) and the $(Zn_{0.58}Cd_{0.42})Se$ HNCs (sample S150−220) consist of 5.1 nm/0.25 nm and 4.6 nm/0.5 nm core/shell structures, respectively. In contrast, the product NCs obtained by carrying out the Zn^{2+} for Cd^{2+} cation exchange reaction directly at 220 °C (Figure 6F) and 200 °C (Figure 6G), *i.e.*, without intermediate heating at lower temperatures, consist of $(Zn_{1-x}Cd_x)Se$ gradient alloy NCs.

Interestingly, extracting sample S150−220 from the reaction mixture, purifying it, and subsequently heating it to 250 °C for 20 min converts the $(ZnSe)_{0.6}/(CdSe)_{0.4}$ core/shell HNCs into $(Zn_{0.6}Cd_{0.4})Se$ homogeneous alloy NCs with shape preservation (Figure 6H and SI, Table S1 and Figure S11). Since carrying out the Zn^{2+} for Cd^{2+} exchange reaction at 250 °C leads to (Zn,Cd)Se homogeneous alloy NCs, this observation shows that fast Cd−Zn interdiffusion occurs at 250 °C, independently of the starting situation (*i.e.*, ZnSe NCs in Cd-containing solution or ZnSe/CdSe core/shell HNCs). Formation of $(Zn_{1-x}Cd_x)Se$ alloy NCs by thermal annealing of CdSe/ZnSe core/shell HNCs has been studied in detail in recent years[10,11,13] and shown to occur at temperatures above 270 °C for HNCs in the 5 to 8 nm size range, with shape and size preservation. The conversion of CdSe/ZnSe core/shell HNCs to homogeneous $(Zn_{1-x}Cd_x)Se$ alloy NCs occurs gradually, through gradient $(Zn_{1-x}Cd_x)Se$ alloy NCs. This is reflected in a gradual shift of the optical transitions until the values for the fully homogeneous alloy are reached.[10,11,13] The time scale for completion ranges from a few minutes to a few hours,

depending on the temperature (270−360 °C) and total HNC size (higher temperatures and/or smaller sizes lead to faster interdiffusion).[10,11,13] The activation energy for the Cd−Zn interdiffusion has been determined to be 152 kJ/mol,[11] which is higher than the bond strength of ZnSe (*viz.*, 136 kJ/mol),[38] but lower than that of CdSe (*viz.*, 310 kJ/mol).[38] In the present case, the Cd−Zn interdiffusion and alloying are observed at lower temperatures (*viz.*, 250 °C) than the minimum temperature reported for CdSe/ZnSe core/shell HNCs (*viz.*, 270 °C),[10] suggesting lower activation energies. This may be ascribed to the lower bond dissociation energy of ZnSe,[38] which makes solid-state diffusion faster in ZnSe NCs than in CdSe NCs, as will be discussed in the mechanism section below. It may thus be expected that ZnSe/CdSe core/shell HNCs will have lower alloying temperatures than the CdSe/ZnSe core/shell HNC analogues.

Carrier Localization Regime and Optical Properties of NCs in the ZnSe−CdSe System. Nanocrystals based on the ZnSe−CdSe combination can have various elemental distribution profiles, of which two extremes can be distinguished: ZnSe/CdSe (or CdSe/ZnSe) core/shell HNCs with a well-defined heterointerface, and (Zn,Cd)Se homogeneous alloy NCs, where Zn and Cd are randomly distributed throughout the cation sites, forming a fully homogeneous solid solution. Gradient alloy (Zn,Cd)Se NCs form a seamless transition between these two extremes. As a result, the optical properties of ZnSe−CdSe NCs can be continuously tuned from those of core/shell HNCs to those of homogeneous alloy NCs, with preservation of the total volume and composition of the NC. The present work provides an interesting illustration of this wide tunability space.

The results presented above clearly show that samples S150 and S150−220 consist of ZnSe/CdSe core/shell HNCs with the same total diameter (5.6 nm), but different core and shell dimensions and, consequently, different compositions (*viz.*, $Zn_{0.74}Cd_{0.26}Se$ and $Zn_{0.58}Cd_{0.42}Se$, respectively). The ZnSe/CdSe core/shell HNCs produced by cation exchange at 150 °C consist of a 5.1 nm ZnSe core overcoated with a 0.25 nm thick CdSe shell, while sequential heating (150 °C followed by 220 °C) yielded thicker CdSe shells (0.5 nm) over smaller (4.6 nm diameter) ZnSe cores (Figure 6A−E), since the in-growth of the CdSe shell by Zn^{2+} for Cd^{2+} cation exchange occurs at the expense of the ZnSe NC core. In contrast, carrying out the cation exchange reaction directly at 200 °C (Figure 6G) and 220 °C (Figure 6F) resulted in (Zn,Cd)Se gradient alloy NCs, while 250 °C produced $(Zn_{0.36}Cd_{0.64})Se$ homogeneous alloy NCs (Figure 6H). The spectral shift to lower energies reflects both the increase of the Cd content and the elemental distribution profile of the (Zn,Cd)Se product NCs. In the following, we will discuss the optical properties of the product (Zn,Cd)Se NCs in detail, starting with the general trends.

The trend observed in the PL QYs (Figure 4) can be attributed to the reaction temperatures, rather than the composition and/or elemental distribution profile of the product (Zn,Cd)Se NCs. As discussed above, sufficiently high temperatures are needed in the steady state to allow the annealing of the defects created by the cation exchange. For this reason, the PL QY is lowest (2%) for reactions carried out at 150 °C, improving as the reaction temperature increases (21% at 200 °C and 80% at 220 °C). The lower PL QY observed for the (Zn,Cd)Se NCs produced at 250 °C (40%) may be attributed to the faster cation exchange rates at this temperature, which resulted in shape deformation (Figure 5D) and likely also a higher concentration of defects. This suggests that 220 °C is the optimum annealing temperature. This reasoning is corroborated by the observation of a broad and relatively weak band at lower energies with respect to the band-edge PL peak in the spectra of the (Zn,Cd)Se NCs obtained at lower reaction temperatures (S150, S200, and S150−220). This band can be ascribed to radiative recombination in trap states,[36] which confirms that the annealing of defects is not effective at lower temperatures (≤200 °C). The observation of trap-PL for sample S150−220, despite its high PL QY (*viz.*, 50%), can be attributed to insufficient annealing time, since this sample was heated at 220 °C for only 5 min. In contrast, sample S220, with a PL QY of 80% and no trap-PL, was heated for 80 min at 220 °C. It is interesting to note that the PL QY of S150−220 is 75%, if the trap-PL band is taken into account. It should also be pointed out that the PL QYs of the most efficient (Zn,Cd)Se NC samples prepared in the present work (*viz.*, S150−220, S220, and S250) are comparable to those reported for efficient CdSe QDs,[36] CdSe-based core/shell HNCs,[1] ZnSe/CdSe core/shell HNCs,[9] and (Zn,Cd)Se gradient[13] and homogeneous alloy NCs.[10]

The shift of the optical transitions of the (Zn,Cd)Se NCs to lower energies is accompanied by a broadening of the absorption and PL peaks. This broadening is easier to quantify in the full-width at half-maximum of the PL peaks, which increases from 108 meV for the parent ZnSe NCs to 120 meV for S150, 210 meV for S150−220, 180 meV for S200, 170 meV for S220, and 130 meV for S250. A similar trend is observed for the nonresonant Stokes shift, which reaches a maximum for S150−220 and then decreases again (*viz.*, 81 meV for the parent ZnSe NCs, 83 meV for S150, 134 meV for S150−220, 90 meV for S220, and 100 meV for S250). The increase observed in the spectral bandwidths and in the Stokes shift may be ascribed to a combination of extrinsic and intrinsic factors. The extrinsic contribution originates from inhomogeneous broadening due to composition fluctuations within the ensemble of product $(Zn_{1-x}Cd_x)Se$ NCs. The intrinsic contribution reflects the increase of both the homogeneous linewidths and the resonant Stokes shift that result from

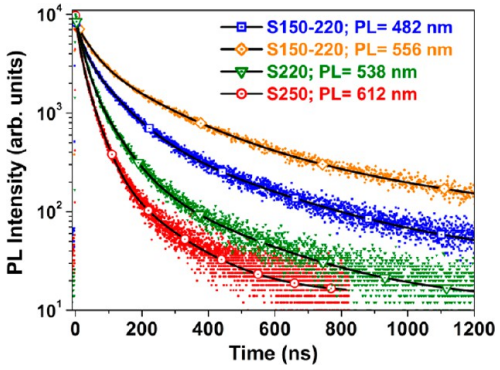

Figure 7. PL decay curves of (Zn,Cd)Se NCs obtained by Zn^{2+} for Cd^{2+} exchange in 5.6 nm ZnSe NCs at different temperatures: 220 °C (sample S220); 250 °C (sample S250); and two consecutive temperatures (150 °C followed by 220 °C, sample S150−220). The solid lines are three-exponential fits to the PL decay data (see SI, Figure S13 for a representative example). The decay constants are given in Table 2. The PL spectra of these samples are shown in Figure 4. The two different PL wavelengths monitored for S150−220 correspond to the band-edge PL (482 nm) and trap-PL (556 nm). Representative TEM images and EELS chemical distribution profile maps of these samples are presented in Figures 5 and 6, respectively.

the reduction of the electron−hole wave function overlap due to partial spatial separation of the charge carriers.[39] The extrinsic contribution is likely to dominate, preventing the observation of trends due to the intrinsic contribution. Previous work on colloidal CdTe/CdSe core/shell HNCs has established that the gradual separation of the electron and hole wave functions results in a progressive shift of the optical transitions to lower energies, accompanied by an increase in the exciton radiative lifetimes.[39] The onset of the type-II localization regime is manifested in the loss of structure in the absorption spectrum and a simultaneous increase in both the Stokes shift values and transition linewidths.[39] It is thus clear that the trends presently observed in the fwhm and Stokes shift values cannot be properly analyzed without taking into account the evolution of the PL decay times.

The PL decay curves of three representative samples of (Zn,Cd)Se NCs (S150−220, S220, and S250) are presented in Figure 7. The PL decay transients are multiexponential and could be well-fit using a three-exponential decay function ($\chi^2 = 1$, in all cases; see SI, Figure S13 for an example). The quality of the biexponential fits was lower ($\chi^2 \approx 1.2-1.4$), primarily due to higher residuals at early decay times (SI, Figure S13). The decay constants obtained from the three-exponential fits are collected in Table 2. A sample of $Zn_{0.67}Cd_{0.33}Se$ homogeneous alloy NCs is also presented. This sample was kindly supplied by X. Zhong and W. Knoll (Max Planck Institute for Polymer Research, Mainz, Germany) and has been prepared by thermal annealing of CdSe/ZnSe core/shell HNCs.[10] Table 2 also includes the exciton lifetimes reported in the literature for ZnSe QDs,[9] CdSe QDs,[35] and ZnSe/CdSe core/shell HNCs.[9]

TABLE 2. Photoluminescence (PL) Quantum Yields (QYs) and PL Decay Constants of $(Zn_{1-x}Cd_x)Se$ NCs Obtained by Zn^{2+} for Cd^{2+} Cation Exchange in 5.6 nm Diameter ZnSe NCs at Different Temperatures[a]

sample	QY (%)	λ_{em} (nm)	τ_1 (ns)	A_1 (%)	τ_2 (ns)	A_2 (%)	τ_3 (ns)	A_3 (%)
S150[b]	2	463	3	82	20	16	99	2
		577[tr]	5	63	30	30	158	7
S150−220[c]	50	482	23	45	89	45	337	10
	75[tot]	556[tr]	44	51	190	41	746	8
S220[d]	80	538	20	64	65	33	273	3
S250[e]	40	612	11	52	36	45	148	3
$Zn_{0.67}Cd_{0.33}Se$[f]	70	495	11.5	84	33	15	188	1
ZnSe QDs[9]	60−80	430	20					
		460	33					
CdSe QDs[35]	50−80	480	13					
		530	16					
		612	26					
ZnSe/CdSe[9g]	60−80	430			27−34			
		480			25−69			
		530			36−70			
		600			39−78			

[a] A sample of $(Zn_{0.67}Cd_{0.33})Se$ homogeneous alloy NCs obtained by alloying CdSe/ZnSe core/shell HNCs is also presented.[10] Literature data on ZnSe QDs,[9] CdSe QDs,[35] and ZnSe/CdSe core/shell HNCs[9] are included for comparison. The superscript tot indicates the QY that is obtained if trap-PL is also included. λ_{em} = monitored emission wavelength. The superscript tr indicates that the emission is assigned to trap-PL. τ_i, A_i = Parameters obtained from a best fit of the experimental PL decay curves to a three-exponential decay function: τ_i is the decay constant, A_i is the fractional amplitude of τ_i at $t = 0$. Representative examples of two- and three-exponential fits, including goodness of fit criteria (reduced χ^2 and residuals), are shown in the Supporting Information (Figure S13). [b] $(ZnSe)_{0.74}/(CdSe)_{0.26}$ core (5.1 nm)/shell (0.25 nm) HNC. Optical spectra provided in Figure 4. [c] $(ZnSe)_{0.58}/(CdSe)_{0.42}$ core (4.6 nm)/shell (0.5 nm) HNC. Optical spectra provided in Figure 4. EELS chemical distribution profile map in Figure 6A−E; PL decay curve in Figure 7. [d] $Zn_{0.56}Cd_{0.44}Se$ gradient alloy NC. Optical spectra provided in Figure 4. EELS chemical distribution profile map in Figure 6F; PL decay curve in Figure 7. [e] $Zn_{0.36}Cd_{0.64}Se$ homogeneous alloy NC. Optical spectra provided in Figure 4. EELS chemical distribution profile map in Figure 6H; PL decay curve in Figure 7. [f] Homogeneous alloy NCs, $d = 7.5 \pm 0.6$ nm. Sample kindly supplied by X. Zhong and W. Knoll (Max Planck Institute for Polymer Research, Mainz, Germany) (see ref 10 for details). [g] ZnSe/CdSe core/shell HNCs of various core diameters and shell thicknesses, but emitting at the same wavelength. The fit of the experimental decay transients was performed only in the range of 50 to 140 ns. Therefore, we assume that the decay constants reported in ref 9 are equivalent to τ_2 in the present work.

The observation of two coexisting radiative decay channels has been recently reported for CdTe/CdSe HNCs in the type-I[1/2] and type-II regimes[39,40] and was ascribed to exciton states with different degrees of spatial localization (*viz.*, a state with larger electron−hole overlap and faster radiative decay rate, and a state with larger spatial separation and slower radiative decay rate).[39] Emission from two different exciton states with different degrees of electron localization has also been recently reported for single CdSe/CdS core/shell tetrapods.[41] In the present case, the observation of three radiative decay channels can be

ascribed to two exciton states with different degrees of spatial localization (lifetimes τ_1 and τ_2) and trap-assisted radiative recombination (τ_3). This interpretation is supported by the fact that the contribution of τ_3 is negligible for samples that show no trap-PL (S220, S250 and $Zn_{0.67}Cd_{0.33}Se$). Interestingly, the trend for all three lifetimes is consistent with that reported above for the fwhm and Stokes shift values: the lifetimes are longest for S150−220 (core/shell HNCs) and decrease from S150−220 to S220 (gradient alloy NCs) and from these to S250 and $Zn_{0.67}Cd_{0.33}Se$ (homogeneous alloy NCs). This suggests that the spatial separation between the electron and hole wave functions is maximum in the ZnSe/CdSe core/shell HNCs and gradually decreases as the homogeneous alloy limit is reached. The type-II localization regime can however be excluded, since the featureless absorption tail characteristic of spatially indirect excitons[39] is absent in the absorption spectra of all samples. As will be shown below, the observations presented above can be rationalized by considering that S150−220 is in the type-$I^{1/2}$ regime, while the homogeneous alloy NCs are analogous to single compound NCs, for which the carrier localization regimes become meaningless, as the wave functions of both carriers probe the whole volume of the NC. The gradient alloy NCs can then be seen as gradually evolving from the type-$I^{1/2}$ regime toward the homogeneous alloy electronic structure.

The spatial distributions of electron and hole wave functions as a function of the core and shell dimensions in ZnSe/CdSe core/shell HNCs have been theoretically analyzed by Klimov and co-workers, using a two-band, effective-mass approximation approach.[9] The authors concluded that thin CdSe shells ($\leq$1 to 1.1 nm, depending on the core diameter) would yield type-I HNCs with both electron and hole localized in the ZnSe core, while thick CdSe shells ($\geq$1.4 to 1.7 nm, depending on the core diameter) would yield inverted type-I HNCs in which electron and hole localize in the CdSe shell. Intermediate shell thicknesses would result in HNCs in the type-$I^{1/2}$ regime (electron in CdSe shell, hole delocalized over the entire volume of the HNC).[2,9] However, the experimental results reported in ref 9 were not fully consistent with the theoretical expectations, since the exciton lifetimes of type-I and inverted type-I ZnSe/CdSe core/shell HNCs were longer than those observed for single-composition ZnSe QDs or CdSe QDs emitting at the same wavelength (Table 2). Moreover, the wide range of observed lifetimes for any given detection wavelength (Table 2) precluded the identification of clear trends in the data.[9]

Another limitation of the analysis reported in ref 9 is that the PL decay curves were fit only in the 50 to 140 ns range, which renders the results inconclusive with respect to whether or not the decay transients were truly single exponential. For this reason, we assume that the lifetimes reported in ref 9 are equivalent to τ_2 in the present work. Bearing this assumption in mind, one can see that the lifetimes observed in the present work for sample S150−220 (4.6 nm/0.5 nm ZnSe/CdSe core/shell HNCs) are in good agreement with the upper limit of the values reported in ref 9 for type-$I^{1/2}$ ZnSe/CdSe core/shell HNCs emitting at comparable wavelengths. The lifetimes observed for sample S150−220 are also consistent with those reported for type-$I^{1/2}$ CdTe/CdSe core/shell HNCs (*viz.*, τ_1 = 22−30 ns; τ_2 = 38−80 ns; depending on the CdSe volume fraction).[39] Considering also the trends in the fwhm and Stokes shift discussed above, it becomes clear that S150−220 is in the type-$I^{1/2}$ localization regime (hole wave function delocalized over the whole HNC volume and electron wave function centered in the CdSe shell). It is interesting to note that the lifetimes obtained while monitoring the trap-PL of S150−220 (Table 2) are substantially longer than those extracted from the decay of the band-edge PL, which is consistent with carrier localization in shallow traps.

To probe the amplitude of the hole wave function at the surface of the ZnSe/CdSe HNCs, an excess of hexanedithiol (HdT) was added to S150−220. For comparison, HdT was also added to S220. Alkylthiols are very efficient hole traps on both CdSe and ZnSe QDs, thereby quenching the excitonic emission.[8,42] Nevertheless, thiols have been shown to be unable to induce PL quenching on HNCs in which the hole is confined to the core, such as type-$I^{1/2}$ and type-II CdTe/CdSe HNCs.[39] In the present case, the PL is completely quenched for both the ZnSe/CdSe core/shell HNCs (S150−220) and the (Zn,Cd)Se gradient alloy NCs (S220) (SI, Figure S14), confirming that the hole wave function reaches the NC surface in both cases. The delocalization of the hole wave function over the whole volume of ZnSe/CdSe core/shell HNCs has also been experimentally demonstrated by measurements of the excitonic Zeeman splittings for a series of $Zn_{1-x}Mn_xSe$/CdSe and $Zn_{1-x}Mn_xSe$/ZnSe core/shell HNCs.[43]

The PL decay of S150 (5.1 nm/0.25 nm ZnSe/CdSe core/shell HNCs) is dominated by nonradiative recombination, as expected considering the low PL QY of this sample (*viz.*, 2%), and can therefore not be used to detect changes in the carrier localization regime, since it cannot provide information over the radiative decay rates. Nevertheless, the fact that the fwhm and Stokes shift values of S150 are essentially the same as those of the parent ZnSe NCs can be interpreted as evidence that this sample is in the type-I regime. However, the substantial shift of both absorption and PL transitions to lower energies with respect to the parent ZnSe NCs demonstrates that the confinement potential is not sufficiently large to prevent the electron and hole wave functions from reaching the surface. In fact, a key characteristic of ZnSe/CdSe core/shell HNCs is that shell growth results in a substantial red shift of all the

exciton transitions.[9,43] This shift to lower energies has been ascribed to an increase in the effective exciton volume due to leakage of both electron and hole wave functions into the shell.[9] However, the shift observed for (formally) type-I ZnSe/CdSe core/shell HNCs (*e.g.*, −80 meV for S150, shell volume fraction ∼25%) is much larger than that observed for other type-I core/shell HNCs, such as CdSe/ZnS and CdSe/ZnSe (*e.g.*, −15 and −20 meV, for 25% shell volume fractions over 4 nm cores),[1] or even type-I$^{1/2}$ HNCs, such as CdSe/CdS (−50 meV, for 25% shell volume fractions over 4 nm cores).[1]

The present results provide deeper insight into the nature of the exciton red shift in ZnSe/CdSe core/shell HNCs, since the total HNC volume is preserved, as the CdSe shell grows at the expense of the ZnSe NC core. Our work thus clearly demonstrates that the large red shifts observed upon CdSe shell growth around ZnSe NC cores (either by heteroepitaxial overgrowth or cation exchange in-growth) are not merely caused by the extension of the wave functions into the shell volume, but reflect mixing of CdSe character into the electron wave function of the ZnSe NCs. Due to its much smaller effective mass, the electron confinement energy is larger than that of the holes.[14] Therefore, the decrease induced in the potential energy of the electron by partial mixing of CdSe character into the conduction band levels will lead to a substantial change in the NC energy gap[43] and should enhance the shift of the electron wave function into the CdSe shell, thus reducing the critical shell thickness for the onset of the type-I$^{1/2}$ localization regime.

The thermally induced conversion of CdSe/ZnSe core/shell HNCs into (Zn,Cd)Se homogeneous alloy NCs, with preservation of the composition and total volume, has clearly demonstrated that the optical properties can be continuously tuned from one extreme to the other *via* gradient alloy NCs.[10,13] As pointed out above, the substantial differences between the optical properties of S150−220 (4.6 nm/0.5 nm $(ZnSe)_{0.58}/(CdSe)_{0.42}$ core/shell HNCs) and S220 (5.8 nm diameter $Zn_{0.56}Cd_{0.44}Se$ gradient alloy NCs), despite their similar sizes and compositions, provide a clear illustration of the profound impact of the elemental distribution profiles on the nature and localization of the hole and electron wave functions. The thiol addition experiments discussed above (SI, Figure S14) have shown that the hole wave function is delocalized over the whole volume of the NC in both cases. The differences between the optical properties of the two samples must thus be due to changes in the localization and nature of the electron wave function.

The shortening of the lifetimes from S150−220 to S220 (Table 2) indicates an increase of the electron−hole overlap, which can be attributed to a shift of the electron wave function maximum toward the center of the NC, where the maximum amplitude of the hole wave function is located.[14] This can be ascribed to the more diffuse interface between Zn-rich and Cd-rich regions in $(Zn_{1-x}Cd_x)Se$ gradient alloy NCs, which results in a gradually changing potential, which softens the confinement potential for both electron and hole.[14] Moreover, the intermixing between Cd and Zn leads to a change in the nature of the electron and hole wave functions, which acquire increasingly larger CdSe character in the case of alloying of ZnSe/CdSe core/shell HNCs (resulting in a gradual red shift of all the exciton transitions) or increasingly larger ZnSe character in the case of alloying of CdSe/ZnSe core/shell HNCs (resulting in a gradual blue shift of all the exciton transitions). The loss in confinement potential for both carriers causes an additional shift to lower energies. The smoother the (Zn,Cd) chemical gradient becomes, the softer the confinement potential and the stronger the mixing between CdSe and ZnSe wave functions, until the limit of the fully homogeneous $(Zn_{1-x}Cd_x)Se$ alloy is reached (electron and hole wave functions delocalized over the whole NC). The gradual change in the localization and nature of the electron and hole wave functions will be reflected in a gradual shortening of the exciton radiative lifetimes due to the increase in the electron−hole overlap, as indeed observed in Table 2.

It is interesting to note that the PL decay constants of the two samples of homogeneous alloy NCs are remarkably similar (Table 2), despite their different compositions and PL wavelengths (*viz.*, $Zn_{0.36}Cd_{0.64}Se$ and $Zn_{0.67}Cd_{0.33}Se$ emitting at 612 and 495 nm, respectively). This suggests that the radiative lifetime of a direct exciton in (Zn,Cd)Se homogeneous alloy NCs is ∼11 ns. This is faster than the radiative lifetimes of CdSe and ZnSe QDs, but is comparable to the radiative lifetimes recently calculated by Efros and co-workers for a trion (*i.e.*, two holes and one electron) in (Zn,Cd)Se gradient alloy NCs (*viz.*, 7−9 ns).[14] The possibility of observing the radiative recombination of a charged exciton (trion) in these systems was attributed to greatly reduced Auger recombination rates as a result of the soft confinement potential.[14] The similarity between the τ_2 values of S250 and $Zn_{0.67}Cd_{0.33}Se$ NCs (Table 2) and the radiative lifetimes of ZnSe and CdSe QDs suggests the intriguing possibility that the two lifetimes (τ_1 and τ_2) observed for (Zn,Cd)Se homogeneous alloy NCs can be ascribed to the radiative recombination of charged and neutral excitons, respectively. Nevertheless, further work is needed before the multiple radiative decay channels observed in the present work for ZnSe/CdSe core/shell HNCs and (Zn,Cd)Se alloy NCs can be unambiguously assigned. As extensively demonstrated for the prototypical case of CdSe QDs,[7,44−46] studies of the temperature dependence of the exciton lifetimes and of inter- and intraband relaxation processes should provide invaluable insights on the energy level structure of these systems.

Mechanism for the Cation Exchange in ZnSe NCs. The results discussed above clearly show that the Zn^{2+} for Cd^{2+} cation exchange (CE) in ZnSe NCs is a thermally activated isotropic process. Therefore, the reaction temperature can be used as a sensitive parameter to tune the CE kinetics and consequently tailor both the composition and the elemental distribution profile of the product $(Zn_{1-x}Cd_x)Se$ NCs. The initial exchange is fast, but quickly slows down, and eventually reaches a steady state. The CE efficiency (*i.e.*, fraction of Cd^{2+} ions originally in solution, Cd_{sol}, that is incorporated in the ZnSe NCs) when the steady state is reached increases with the temperature. The CE efficiency depends also on the Cd_{sol}/ZnSe ratio, and therefore the system can be taken out of the steady state upon addition of more Cd-oleate, although the CE efficiency slowly decreases with the extent of the exchange (*i.e.*, larger Cd_{sol}/ZnSe ratios are needed to drive the exchange further).

Interestingly, in contrast to other isovalent CE reactions (*e.g.*, Pb^{2+} for Cd^{2+} in PbX NCs),[21] the elemental distribution profile of the product (Zn,Cd)Se NCs can be controlled by the reaction temperature: 150 °C produces ZnSe/CdSe core/shell HNCs, 200 and 220 °C produce $(Zn_{1-x}Cd_x)Se$ gradient alloy NCs, while 250 °C results in $(Zn_{1-x}Cd_x)Se$ homogeneous alloy NCs. Remarkably, sequential heating (150 °C followed by 220 °C) leads to ZnSe/CdSe core/shell HNCs with thicker shells, rather than $(Zn_{1-x}Cd_x)Se$ gradient alloy NCs. Despite the larger lattice parameters of CdSe with respect to those of ZnSe (*viz.*, a_0= 6.077 and 5.668 Å, respectively, for zinc-blende structure), the Se sublattice remains unaffected at low temperatures (≤220 °C) (SI, Figure S8). However, the product (Zn,Cd)Se NCs experience expansion and reorganization at sufficiently high temperatures (≥220 °C) and/or under fast exchange rates.

To explain these observations, we will propose below a mechanism for the Zn^{2+} for Cd^{2+} exchange in ZnSe NCs. The essential aspects of this mechanism are schematically illustrated in Figure 8. Cation exchange reactions consist of a number of inherently linked elementary kinetic steps.[19] The thermodynamic driving force is determined by the energy balance of the overall reaction. Since the elementary steps proceed in a concerted manner, the energy input or output involved in each step is important.[19] In the present case, the overall cation exchange reaction can be written as

$$x\text{Cd(Oleate)}_{2(sol)} + [\text{ZnSe}]_{NC} \rightarrow x\text{Zn(Oleate)}_{2(sol)} + [(Zn_{1-x}Cd_x)Se]_{NC}$$

This reaction involves four simultaneous chemical processes, since two compounds dissociate (*viz.*, [ZnSe] units and $Cd(oleate)_2$), while two new compounds form (*viz.*, [CdSe] units and $Zn(oleate)_2$). This process is energetically driven both by the larger Cd−Se bond strength with respect to that of Zn−Se (310 *versus* 136 $kJ \cdot mol^{-1}$, respectively)[38] and by the larger stability of $Zn(oleate)_2$ with respect to $Cd(oleate)_2$.[1,47] To qualitatively discriminate the relative importance of the [ZnSe]−[CdSe] and $Cd(oleate)_2$−$Zn(oleate)_2$ partial energy balances to the overall CE energy balance, two control experiments were carried out in which $Cd(oleate)_2$ was replaced by either $Cd(hexanoate)_2$ or Na(oleate), under otherwise identical conditions at 220 °C. The outcome of these control experiments is summarized in Figures 9 and S15 (SI).

It is clear that Na(oleate) does not react (Figure 9), demonstrating that the formation of $Zn(oleate)_2$ alone is not enough to drive the exchange reaction (in this case both Na(oleate) and Na_2Se are less stable than the Zn analogues). The lack of reactivity of Na-oleate implies that the energy gain from forming the Cd−Se bond is crucial for the overall energy balance. Interestingly, the cation exchange reaction using $Cd(hexanoate)_2$ as the metal precursor reaches the steady state with a much lower exchange efficiency than when $Cd(oleate)_2$ is used (Figure 9). The reactivity of metal carboxylate salts is known to increase with decreasing chain length,[1] due to a combination of faster diffusion rates, less steric hindrance when bound to surface sites, and lower thermal stability (*e.g.*, $Zn(acetate)_2$ decomposes at 300 °C, while $Zn(oleate)_2$ decomposes at 400 °C).[48] The lower exchange efficiency achieved when using the more reactive $Cd(hexanoate)_2$ complex shows that the energy gain upon formation of $Zn(hexanoate)_2$ is not enough to compensate the energy lost by breaking the Zn−Se bond, despite lower energy costs to break the Cd−hexanoate bonds and the energy gained upon formation of the Cd−Se bond. This suggests that the rate-limiting step in the Zn^{2+} for Cd^{2+} exchange reaction is likely the formation of a surface-activated complex in which the new bonds (*viz.*, Cd−Se and Zn−carboxylate group) begin to form, while the existing bonds (*viz.*, Zn−Se and Cd−carboxylate group) weaken. This observation also implies that diffusion of the incoming Cd species toward the parent ZnSe NC surface and diffusion of the product Zn species away from it are not rate-limiting steps and can thus be neglected in the present discussion.

The Zn^{2+} for Cd^{2+} place exchange process discussed above is essentially a surface reaction (Figure 8). In the absence of cation diffusion in the NC, the CE reaction would thus be self-limited and would stop as soon as all surface Zn^{2+} cations had been exchanged by Cd^{2+}. Therefore, two solid-state diffusion fluxes must be set in motion to allow the reaction to proceed: inward diffusion of Cd^{2+} and outward diffusion of Zn^{2+}. Diffusion processes have been investigated in detail in bulk ZnSe.[49] Self-diffusion of Zn^{2+} in ZnSe has been shown to occur *via* neutral Frenkel pairs (*i.e.*, a Zn^{2+} vacancy, V_{Zn}, associated with an interstitial Zn^{2+}, Zn_i).[49] Frenkel pairs are the dominant native defect

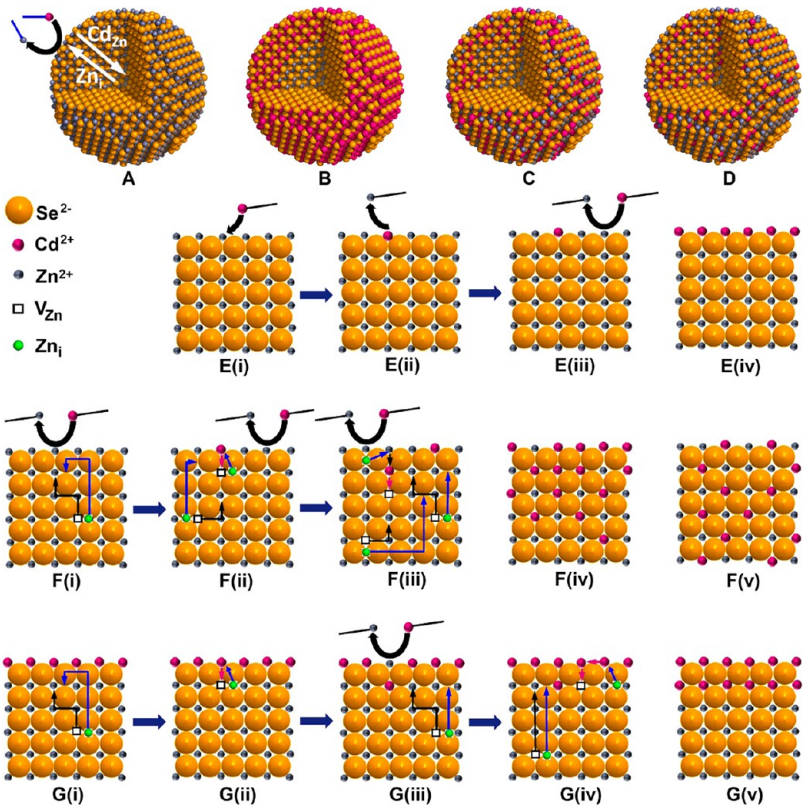

Figure 8. Schematic of the mechanism proposed for the Zn^{2+} for Cd^{2+} cation exchange (CE) in ZnSe NCs. (A) Cartoon depicting the essential kinetic elementary steps in the CE mechanism. Fast CE takes place at the NC surface and is followed by relatively slower thermally activated solid-state cation diffusion. The diffusion is mediated by Frenkel pairs, so that the outward diffusion flux consists of interstitial Zn^{2+} cations (Zn_i), while the incoming Cd^{2+} cations diffuse inwardly by hopping into the Zn^{2+} vacancies that were accompanying the Zn_i (*i.e.*, as Cd_{Zn}). The CE reaction is energetically driven both by the larger Cd−Se bond strength and by the larger stability of $Zn(oleate)_2$. Depending on the CE reaction conditions, ZnSe/CdSe core/shell HNCs (B), $(Zn_{1-x}Cd_x)Se$ gradient alloy NCs (C), or $(Zn_{1-x}Cd_x)Se$ homogeneous alloy NCs (D) are obtained. At low temperatures (150 °C) the concentration of Frenkel pairs (Zn_i−V_{Zn}) is negligible, thereby precluding diffusion within the NC. Cation exchange will then be limited to the NC surface, producing ZnSe/CdSe core/thin shell HNCs [panels E(i) to E(iv)]. At higher temperatures the concentration of Zn_i−V_{Zn} pairs is sufficiently high, and therefore Zn^{2+} for Cd^{2+} exchange at the surface will occur simultaneously with solid-state diffusion processes within the NC [panels F(i) to F(iii)]. Under such conditions, gradient or homogeneous alloy NCs (F(iv) and F(v), respectively) will be obtained, depending on the balance between exchange and diffusion rates. Sequential heating (150 °C followed by 220 °C) leads to ZnSe/CdSe core/thick shell HNCs because the solid state diffusion processes start after the NC surface has been converted to CdSe [G(i) to G(v)].

in bulk ZnSe, owing to the open nature of the zinc-blende structure (one interstitial tetrahedral site and one interstitial octahedral site *per* occupied cationic site), in combination with the small size of the Zn^{2+} cation (*viz.*, 0.60 Å) and relatively weak Zn−Se bonds (136 kJ·mol^{-1}).[38] In the mechanism proposed here (Figure 8), we assume that Frenkel pairs are also the dominant native defect in ZnSe NCs and are responsible for solid-state diffusion within the NC. As will be shown below, this mechanism explains well the observations reported in the present work.

The formation of Frenkel pairs is a strongly temperature-dependent equilibrium process, in which a cation originally at a regular site moves into a vacant interstitial site, leaving a vacancy behind. At any temperature, the concentrations of Zn_i and V_{Zn} are equal and are given by 2 exp($-\Delta H_{Frenkel}/2kT$) ($\Delta H_{Frenkel}$ = formation enthalpy of a Frenkel defect). Both Zn_i and V_{Zn} can move through the solid by hopping from site to site, which requires an activation energy that will vary depending on the nature of the sites involved. The impact of the temperature on the composition and elemental distribution profile of the product $(Zn_{1-x}Cd_x)Se$ NCs obtained by Zn^{2+} for Cd^{2+} exchange in ZnSe NCs can thus be well understood by assuming that the reaction is limited by solid-state diffusion within the NC, since these rates are strongly temperature dependent.

At 150 °C the concentration of Frenkel pairs is negligible, thereby precluding any sizable diffusion within the NC. Therefore, the cation exchange process is limited to the NC surface and stops as soon as the Zn^{2+} cations at the surface are depleted, producing ZnSe/CdSe core/thin shell HNCs (Figure 8E). Indeed, the estimated thickness of the CdSe shell of sample S150 (*viz.*, 0.25 nm) corresponds very well to the Cd−Se bond length (*viz.*, 0.2632 nm) and is thus consistent with a single monolayer of CdSe. At higher temperatures, the concentration of Frenkel pairs is sufficiently

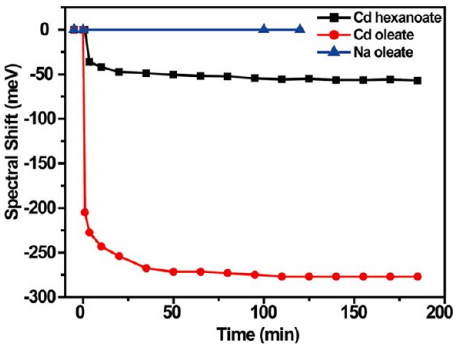

Figure 9. Temporal evolution of the spectral shift observed for the lowest energy absorption transition of product (Zn,Cd)Se NCs obtained by Zn^{2+} for Cd^{2+} cation exchange in 5.6 nm ZnSe NCs at 220 °C using two different Cd precursors (cadmium hexanoate and cadmium oleate). A control experiment in which the Cd precursor was replaced by sodium oleate is also presented. The reaction was driven by a single metal-precursor injection at $t = 0$. All reaction parameters, other than the metal precursor, were identical. The absorption and PL spectra of the NC samples obtained after 120 min of reaction are presented in the SI (Figure S15).

high to allow solid-state diffusion processes to occur (Figure 8A,F,G). The Zn^{2+} cations migrate to the surface as interstitials (Zn_i) and are exchanged by Cd^{2+} cations, which hop to the leftover Zn^{2+} vacancy (V_{Zn}) and thus diffuse inward. The Zn^{2+} for Cd^{2+} place exchange reaction at the surface will thus annihilate both Zn_i and V_{Zn}, shifting the Frenkel equilibrium toward production of more Zn_i–V_{Zn} pairs. Concomitantly, this establishes a concentration gradient that drives the Cd^{2+} flux inward (*via* the V_{Zn}) and the Zn^{2+} flux outward (as Zn_i) (Figure 8). At lower temperatures (*e.g.*, 200 °C) the concentration of Frenkel pairs is lower and the distribution of kinetic energies of the diffusing cations is narrower. Therefore, the diffusion fronts are spatially narrower, resulting in $(Zn_{1-x}Cd_x)Se$ gradient alloy NCs with steeper gradients. As the temperature increases, the width of the diffusion front and of the distribution of kinetic energies are both larger, resulting in $(Zn_{1-x}Cd_x)Se$ gradient alloy NCs with increasingly smoother gradients, until the fully homogeneous alloy limit is reached ($T \geq 240$ °C).

The striking difference between the elemental distribution profiles of samples S220 (gradient alloy NCs, obtained by heating at 220 °C) and S150–220 (ZnSe/CdSe core/shell HNCs, obtained by sequential heating: 150 °C followed by 220 °C) implies that the thin CdSe shell produced by Zn^{2+} for Cd^{2+} exchange at 150 °C spatially narrows both the inward Cd^{2+} flux and the outward Zn_i flux (Figure 8G). This can be ascribed to a combination of factors. Since the Se sublattice remains essentially intact during the Zn^{2+} for Cd^{2+} exchange at low temperatures, the lattice parameters of the parent ZnSe NCs are preserved, despite the larger size of the Cd^{2+} cation. The CdSe shell is thus formed under compressive strain, since the lattice parameters of bulk CdSe are 7% larger than those of bulk ZnSe. This is clearly demonstrated by the fact that the lattice spacings observed in the HR-STEM images of the $(ZnSe)_{0.58}/(CdSe)_{0.42}$ core/shell HNCs (S150–220) (SI, Figure S8) match the values for ZnSe. The high interfacial tension at the ZnSe/CdSe heterointerface imposes additional energy barriers both for the Zn_i diffusion through the CdSe shell and for the Cd^{2+} diffusion into the ZnSe core. The latter process increases the strain field if lattice expansion is prevented, since it leads to a thicker shell with preservation of the lattice parameters of ZnSe. If the cation exchange process is started at 220 °C, the Se-sublattice will be able to (partially) expand to accommodate the larger incoming Cd^{2+} cations, since exchange and diffusion occur simultaneously, thereby preventing the formation of a continuous CdSe surface shell during the fast exchange phase (Figure 8F). In contrast, the presence of the CdSe surface shell formed at 150 °C will prevent the NC expansion at 220 °C, due to the larger Cd–Se bond strength. This results in larger activation energies for the formation of Frenkel defects and also larger thermal stability. It should be noted that the energy barriers imposed by the ZnSe/CdSe heterointerface on diffusion fluxes are nevertheless small, as clearly demonstrated by the formation of (Zn,Cd)Se homogeneous alloy NCs at 250 °C, both by cation exchange and thermally induced Cd–Zn interdiffusion (alloying). This implies that, to fully harvest the potential of the sequential heating strategy to tailor the elemental distribution profiles of (Zn,Cd)Se NCs, one should make sure that all the temperatures used are sufficiently low, unless a fully homogeneous alloy NC with predetermined size and shape is desired.

It is interesting to note that the solid-state diffusion rates observed in the present work are orders of magnitude faster than those in bulk ZnSe. For example, the Zn–Cd interdiffusion coefficient in bulk ZnSe/CdSe heterojunctions is equal to $6.4 \times 10^{-4} \exp(-1.87\ eV/kT)\ cm^2 \cdot s^{-1}$,[49] which gives a negligible interdiffusion coefficient at 220 °C (*viz.*, $\sim 1 \times 10^{-47}\ cm^2.s^{-1}$). This is one of the key characteristics of nanoscale cation exchange and alloying reactions and has been attributed to the larger surface/volume ratio of NCs.[19] On the basis of the cation exchange mechanism discussed above, this observation implies that the activation energies for diffusion and the energy required to form Frenkel pairs are both lower in ZnSe NCs than in bulk ZnSe and are also strongly site-dependent, increasing toward the center of the NC in a radial fashion. This is in line with recent HRTEM and solid state ^{77}Se and ^{67}Zn MAS NMR studies on organically capped colloidal ZnSe NCs[50] and CdSe NCs,[51] which have shown that size- and site-dependent reconstruction occurs in these NCs. Positional reconstruction is global for NCs smaller than 4 nm,[51] but is self-limited to the first few monolayers in larger NCs.[50,51] Further, density functional theory calculations indicate that the

positional reconstruction of the surface atoms creates an electronic perturbation that propagates 6−7 monolayers inward, affecting the bond strength of atoms that otherwise have the exact positional ordering of bulk ZnSe up to their third or fourth coordination spheres.[50] These results imply that the bond strengths in colloidal ZnSe (or CdSe) NCs are smaller than in bulk and increase from the surface to the center of the NC in a depth-dependent and radial fashion,[50,51] in good agreement with the observations and CE mechanism reported in the present work.

CONCLUSIONS

In conclusion, the work presented here reveals that the Zn^{2+} for Cd^{2+} cation exchange in ZnSe NCs is a thermally activated isotropic process. The initial exchange rates are fast, but quickly decrease in time, eventually reaching a steady state. The CE efficiency (*i.e.*, fraction of Cd^{2+} ions originally in solution, Cd_{sol}, that is incorporated in the ZnSe NC) when the steady state is reached increases with the temperature and depends also on the Cd_{sol}/ZnSe ratio. The system can thus be taken out of the steady state upon addition of more Cd-oleate, which causes a quick burst of exchange followed by a new steady state. The CE efficiency slowly decreases with the extent of the exchange (*i.e.*, larger Cd_{sol}/ZnSe ratios are needed to drive the exchange further).

Interestingly, the reaction temperature can be used as a sensitive parameter to tailor both the composition and the elemental distribution profile of the product $(Zn_{1-x}Cd_x)Se$ NCs. At 150 °C ZnSe/CdSe core/shell HNCs are obtained, while higher temperatures (*viz.*, 200 and 220 °C) produce $(Zn_{1-x}Cd_x)Se$ gradient alloy NCs. The concentration gradients within the alloy NCs become increasingly smoother as the reaction temperature increases, until $(Zn_{1-x}Cd_x)Se$ homogeneous alloy NCs are obtained at $T \geq 240$ °C. Remarkably, sequential heating (*i.e.*, 150 °C followed by 220 °C) leads to ZnSe/CdSe core/shell HNCs with thicker shells, rather than $(Zn_{1-x}Cd_x)Se$ gradient alloy NCs. Thermal treatment at 250 °C can be used to convert ZnSe/CdSe core/shell HNCs into $(Zn_{1-x}Cd_x)Se$ homogeneous alloy NCs, while preserving the NC shape and composition. To explain these observations, a mechanism for the Zn^{2+} for Cd^{2+} exchange in ZnSe NCs is proposed, in which fast CE takes place at the NC surface and is followed by relatively slower thermally activated solid-state cation diffusion. The diffusion is mediated by Frenkel pairs, so that the outward diffusion flux consists of interstitial Zn^{2+} cations (Zn_i), while the incoming Cd^{2+} cations diffuse inwardly by hopping into the Zn^{2+} vacancies that were accompanying the Zn_i. The Zn^{2+} for Cd^{2+} exchange reaction in ZnSe NCs is energetically driven both by the larger Cd−Se bond strength and by the larger stability of $Zn(oleate)_2$.

The findings presented here demonstrate that the Zn^{2+} for Cd^{2+} exchange reaction in colloidal ZnSe NCs provides a very sensitive tool to control the compositional distribution profile of (Zn,Cd)Se NCs, while preserving their size and shape. This is crucially important, as it allows the nature and localization of the electron and hole wave functions to be engineered, which in turn makes it possible to tune the optoelectronic properties of the product (Zn,Cd)Se NCs over a wide range. The carrier localization regime has been shown to have a profound impact on a number of photophysical processes (*e.g.*, exciton radiative lifetimes,[8,9,39] exciton−phonon coupling,[52] Auger recombination,[14,53] intraband relaxation,[8] spin relaxation,[40] thermal quenching[54]). This flexibility in engineering the properties of colloidal HNCs and NCs has important consequences for a number of technologies and opens up interesting application possibilities (*e.g.*, lasers,[53] light-emitting diodes,[55] photovoltaic devices,[56] biomedical imaging,[57] luminescent solar concentrators[58]). Our results thus pave the way to the fabrication of ZnSe/CdSe HNCs and $(Zn_{1-x}Cd_x)Se$ alloy NCs in which size, shape, and electron−hole overlap can be tailored to specific needs.

EXPERIMENTAL METHODS

Materials. Cadmium acetate dihydrate ($Cd(Ac)_2 \cdot xH_2O$, 99.99+%), octadecene (ODE, 90%), oleic acid (OA, 90%), and trioctylphosphine (TOP) were purchased from Sigma-Aldrich. Octadecylamine (ODA, >90%), diethylzinc ($Zn(Et)_2$, 98%), and selenium powder (Se, 99.999%) were purchased from Fluka, Strem Chemicals, and Alfa Aesar, respectively. Anhydrous solvents (toluene, hexane, methanol, and acetone) were purchased from Sigma-Aldrich. All reagents were used as purchased, with the exception of ODE and ODA, which were dried and degassed under vacuum (3 h at 120 °C) before use.

Stock Solutions. Stock solutions were prepared in a glovebox under nitrogen (<5 ppm O_2 and H_2O). A 0.4 M $Zn(Et)_2$ stock solution was prepared by dissolving 0.494 g (4 mmol) of $Zn(Et)_2$ in 10 mL of ODE. A 0.4 M Zn-oleate solution was made by dropwise addition of 5.05 mL of OA to a solution of 0.494 g of $Zn(Et)_2$ in 4.95 mL of ODE. This mixture was allowed to react for 5 min at 300 °C and subsequently for 3 h at 120 °C. Cd-oleate stock solution (0.04 M) was prepared by heating a mixture of 0.128 g (0.48 mmol) of $Cd(Ac)_2 \cdot 2H_2O$, 1.2 mL of OA (3.8 mmol), and 10.8 mL of ODE to 280 °C. This Cd-oleate stock solution was subsequently dried and degassed for 3 h at 150 °C. Cd-hexanoate stock solution was prepared using the same procedure used to prepared Cd-oleate, but replacing OA by hexanoic acid. A Se stock solution in TOP (1 M) was prepared by dissolving 0.79 g (10 mmol) of Se powder in 10 mL of TOP.

Parent ZnSe NCs. All syntheses were carried in a glovebox under nitrogen (<5 ppm O_2 and H_2O). This glovebox was also used to store and process the samples. Colloidal ZnSe NCs with 3.7 nm diameter were synthesized following a method reported in the literature,[59] which is based on injecting $Zn(Et)_2$ and TOP-Se in ODA at 265 °C. This method was adapted to yield 5.6 nm diameter ZnSe NCs. Briefly, 2.5 mL of ODE and 0.55 g of ODA were loaded in a reaction flask and heated to 290 °C. At this temperature, 0.5 mL of $Zn(Et)_2$ stock and 1 mL of Se stock were

swiftly injected under stirring. The temperature was allowed to drop to 270 °C, and 5 min after the initial injection, a dropwise addition of 1.5 mL of Zn-oleate stock solution diluted in 3 mL of ODE was started. Another two additions of Zn-oleate (each with the same amount used in the first addition) followed 15 and 25 min after the initial injection. The synthesis was terminated 10 min after the end of the third Zn-oleate addition by removing the heating mantle.

The ZnSe NCs were purified by a hexane/methanol extraction in order to remove unreacted Zn and Se precursors. Extraction was performed by mixing a solution of the crude reaction mixture in anhydrous hexane and anhydrous methanol (1:4:2 volume ratio). The colored top layer containing the NCs was removed. Subsequently, an equal volume of methanol was added to the NC solution layer for a second hexane/methanol extraction step. In total, this purification step was repeated five times, and after the fifth extraction cycle, the NCs were precipitated by adding anhydrous acetone (1:6 volume ratio). The sediment was isolated by centrifugation (3000 rpm, 15 min) and resuspended in anhydrous toluene, yielding a concentrated stock solution. The concentration of this stock solution was determined from the maximum of the lowest energy absorption peak. The molar extinction coefficient of the 3.7 nm diameter ZnSe NCs was taken from the literature (*viz.*, 1.8×10^5 $L \cdot mol^{-1}$ cm^{-1}, for 3.7 nm ZnSe NCs with the lowest absorption peak at 390 nm).[59] The molar extinction coefficient of the 5.6 nm diameter ZnSe NCs (*viz.*, 2.9×10^5 $L \cdot mol^{-1}$ cm^{-1}) was estimated from the value reported for 3.7 nm diameter NCs, assuming that the absorption cross section *per* NC of the 1S → 1S transition of ZnSe quantum dots follows a size dependence similar to that reported for CdSe quantum dots.[35]

(Zn,Cd)Se NC (HNC) Synthesis. Cation exchange reactions were performed by injecting a solution of Cd-oleate (0.04 M) into a solution of purified ZnSe NCs at a preset temperature in a glovebox under nitrogen (<5 ppm O_2 and H_2O). In a typical synthesis, ODA (1.477 g) and ODE (6.3 mL) were loaded in a reaction flask and heated to a preset reaction temperature (150, 200, 220, and 250 °C). When the preset temperature was reached, a ZnSe NC stock solution in toluene (6×10^{-5} mmol of NCs for 5.6 nm NCs and 1×10^{-4} mmol of NCs for 3.7 nm NCs) was injected, and after 15 s a 0.1 mL aliquot was taken from the reaction mixture. Subsequently, 1.5 mL of Cd-oleate stock solution (0.04 M) was injected in three portions of 0.5 mL (at 0, 20, 40 min), with samples being collected 1 min after each injection. The reactions were stopped by removal of the heating mantle, 80 min after the injection of the parent ZnSe NCs. To investigate the effect of the thermal history on the elemental distribution profile, the reaction mixture obtained at the end of the 150 °C treatment was heated (over 20 min) to 220 °C and allowed to react for an additional 5 min. To follow the reaction kinetics in detail, experiments were also carried out by using single injections of 0.5 mL of Cd-oleate and allowing the reaction to progress over longer periods of time (up to 190 min), while periodically collecting aliquots from the reaction mixture. The influence of the precursor was investigated by replacing Cd-oleate by Cd-hexanoate or Na-oleate, while keeping all other variables unchanged at 220 °C. The product (Zn, Cd)Se NCs were purified using the same procedure described above for ZnSe NCs, but with only one extraction cycle.

Optical Spectroscopy: Optical Spectra, PL Quantum Yields, and PL Decay Times. Absorption spectra were measured on a double-beam Perkin-Elmer Lambda 16 UV/vis spectrometer. PL spectra were recorded by an Edinburgh Instruments FLS920 spectrofluorimeter equipped with a 450 W xenon lamp as excitation source and double grating monochromators. Samples for optical measurements were prepared by directly dissolving the crude reaction mixture in anhydrous toluene under nitrogen and stored in sealed cuvettes. All measurements were performed at room temperature.

PL quantum yields were estimated by comparison with a standard, following a previously reported method,[36] as follows:

$$QY = \left(\frac{1 - T_{ST}}{1 - T_X}\right)\left(\frac{\Delta\Phi_X}{\Delta\Phi_{ST}}\right)q_{ST}$$

where T_{ST} and T_X are the transmittances at the excitation wavelength λ_{exc} for the standard and the sample, respectively, and q_{ST} is the quantum yield of the standard. The terms $\Delta\Phi_X$ and $\Delta\Phi_{ST}$ give the integrated emitted photon flux (photons$\cdot s^{-1}$) for the sample and the standard, respectively, upon excitation at λ_{exc}. The excitation wavelength is chosen such that both the sample and the standard are efficiently excited under exactly the same set of instrumental conditions (400 nm in the present case). The values of $\Delta\Phi_X$ and $\Delta\Phi_{ST}$ are determined from the corrected PL spectra. A sample of CdSe/CdS dot core/rod shell heteronanorods (q_{ST} = 45%, determined with an integrating sphere) was used as standard. Toluene was used as the solvent for both the standard and the (Zn,Cd)Se NC samples. The accuracy of the method is ±15%.

PL decay curves were obtained by time-correlated single-photon counting *via* time-to-amplitude conversion, as previously described.[7,39] A pulsed diode laser (EPL-445 Edinburgh Instruments, 379 nm, 55 ps pulse width, 0.2−20 MHz repetition rate) was used as the excitation source. Very low excitation fluences were used (<0.5 nJ/cm^2) in order to avoid multiexciton formation and to keep the ratio of stop to start pulses below 0.04. The raw decay data were fitted to decay functions using a Simplex minimization algorithm implemented in PICOQUANT FLUOFIT 4.4. To allow consistent comparison between different samples, while ensuring that the obtained decay constants were statistically valid, the decay data were fit from I_0 (t = 0) to <1% I_0 (background level) (see SI, Figure S13 for an example). The fit quality was assessed by two criteria: reduced χ^2 (~1.0) and the weighed residuals' autocorrelation function (random distribution of small values).

Transmission Electron Microscopy. Transmission electron microscopy (TEM) and energy dispersive X-ray spectroscopy (EDS) were performed using a Tecnai microscope (FEI TECNAI G2 T20F) operating at 200 kV. Acquisition time for EDS measurements was ~30 s to ~1 min. To ensure that the elemental concentrations were statistically valid and representative of the whole NC ensemble, EDS analyses were performed on wide areas (~10^4−10^5 nm^2), encompassing hundreds to thousands of NCs, and averaged over several observation spots. TEM measurements were carried out on NC samples that had been purified in order to remove the excess of organic molecules and unreacted precursors. Samples for TEM imaging were prepared by dipping a carbon-coated copper (400-mesh) TEM grid into a toluene solution of NCs. The excess liquid was removed by blotting using filter paper.

X-ray Diffraction (XRD). XRD diagrams were obtained by using a PW 1729 Philips diffractometer, equipped with a Cu Kα X-ray source (λ = 1.5418 Å). Samples for XRD analysis were prepared by depositing a concentrated solution of purified NCs on a Si single-crystalline substrate (100 orientation) under inert atmosphere.

High-Resolution Scanning Transmission Electron Microscopy and Electron Energy Loss Spectroscopy. High-angle annular dark-field (HAADF) scanning transmission electron microscopy (STEM) and STEM-electron energy loss spectroscopy (EELS) experiments were performed on a FEI Titan 50−80 cubed microscope fitted with an aberration-corrector for the imaging lens and another for the probe forming lens as well as a monochromator, operated at 120 kV to acquire the data. Spectroscopy experiments were performed on a GIF-QUANTUM spectrometer. The monochromator was not excited in order to increase the signal-to-noise ratio due to the small contribution from the ultrasmall NCs. The STEM convergence semiangle used was ~21.4 mrad.

Conflict of Interest: The authors declare no competing financial interest.

Acknowledgment. The authors acknowledge financial support from the European Union under the 7th Framework Program, FP7 (Integrated Infrastructure Initiative No. 262348 European Soft Matter Infrastructure, ESMI). X.K. and G.V.T. are grateful to the European Research Council for funding under the 7th Framework Program (FP7), ERC grant No. 246791 "COUNTATOMS". The authors are also grateful to F. Pietra (Utrecht University, The Netherlands) for kindly providing a sample of CdSe/CdS dot core/rod shell nanorods and to X. Zhong and W. Knoll (Max Planck Institute for Polymer Research, Mainz,

Germany) for kindly supplying a sample of (Zn,Cd)Se homogeneous alloy NCs.

Supporting Information Available: Elemental composition of product $(Zn_{1-x}Cd_x)Se$ NCs determined by STEM-EDS. TEM images of $(Zn_{1-x}Cd_x)Se$ NCs reheated to 250 °C. HR-STEM images and EELS elemental maps of product $(Zn_{1-x}Cd_x)Se$ NCs obtained by carrying out the Zn^{2+} for Cd^{2+} exchange reaction at different temperatures (150, 150−220, 200, 220, 250 °C). Temporal evolution of the spectral shift and PL QYs for $(Zn_{1-x}Cd_x)Se$ NCs prepared at 150 and 220 °C. Absorption spectra of ZnSe NCs heated at various temperatures. Absorption and PL spectra of product $(Zn_{1-x}Cd_x)Se$ NCs prepared with and without excess oleic acid and after thiol addition. Examples of two- and three-exponential fits to PL decay curves of $(Zn_{1-x}Cd_x)Se$ NCs. This material is available free of charge *via* the Internet at http://pubs.acs.org.

REFERENCES AND NOTES

1. Donega, C. d. M. Synthesis and Properties of Colloidal Heteronanocrystals. *Chem. Soc. Rev.* **2011**, *40*, 1512–1546.
2. Ivanov, S. A.; Piryatinski, A.; Nanda, J.; Tretiak, S.; Zavadil, K. R.; Wallace, W. O.; Werder, D.; Klimov, V. I. Type-II Core/Shell CdS/ZnSe Nanocrystals: Synthesis, Electronic Structures, and Spectroscopic Properties. *J. Am. Chem. Soc.* **2007**, *129*, 11708–11719.
3. Acharya, K. P.; Khnayzer, R. S.; O'Connor, T.; Diederich, G.; Kirsanova, M.; Klinkova, A.; Roth, D.; Kinder, E.; Imboden, M.; Zamkov, M. The Role of Hole Localization in Sacrificial Hydrogen Production by Semiconductor-Metal Heterostructured Nanocrystals. *Nano Lett.* **2011**, *11*, 2919–2926.
4. Xie, R.; Zhong, X.; Basché, T. Synthesis, Characterization, and Spectroscopy of Type-II Core/Shell Semiconductor Nanocrystals with ZnTe Cores. *Adv. Mater.* **2005**, *17*, 2741–2745.
5. Chin, P. T. K.; Donega, C. d. M.; van Bavel, S. S.; Meskers, S. C. J.; Sommerdijk, N. A. J. M.; Janssen, R. A. J. Highly Luminescent CdTe/CdSe Colloidal Heteronanocrystals with Temperature Dependent Emission Color. *J. Am. Chem. Soc.* **2007**, *129*, 14880–14886.
6. Reiss, P.; Bleuse, J. L.; Pron, A. Highly Luminescent CdSe/ZnSe Core/Shell Nanocrystals of Low Size Dispersion. *Nano Lett.* **2002**, *2*, 781–784.
7. Donega, C. d. M.; Bode, M.; Meijerink, A. Size- and Temperature-Dependence of Exciton Lifetimes in CdSe Quantum Dots. *Phys. Rev. B* **2006**, *74*, 085320.
8. Pandey, A.; Guyot-Sionnest, P. Slow Electron Cooling in Colloidal Quantum Dots. *Science* **2008**, *322*, 929–932.
9. Balet, L. P.; Ivanov, S. A.; Piryatinski, A.; Achermann, M.; Klimov, V. I. Inverted Core/Shell Nanocrystals Continuously Tunable between Type-I and Type-II Localization Regimes. *Nano Lett.* **2004**, *4*, 1485–1488.
10. Zhong, X.; Han, M.; Dong, Z.; White, T. J.; Knoll, W. Composition-Tunable $Zn_xCd_{1-x}Se$ Nanocrystals with High Luminescence and Stability. *J. Am. Chem. Soc.* **2003**, *125*, 8589–8594.
11. Sung, Y.-M.; Lee, Y.-J.; Park, K.-S. Kinetic Analysis for Formation of $Cd_{1-x}Zn_xSe$ Solid-Solution Nanocrystals. *J. Am. Chem. Soc.* **2006**, *128*, 9002–9003.
12. Protiere, M.; Reiss, P. Highly Luminescent $Cd_{1-x}Zn_xSe$/ZnS Core/Shell Nanocrystals Emitting in the Blue-Green Spectral Range. *Small* **2007**, *3*, 399–403.
13. Panda, S. K.; Hickey, S. G.; Waurisch, C.; Eychmuller, A. Gradated Alloyed CdZnSe Nanocrystals with High Luminescence Quantum Yields and Stability for Optoelectronic and Biological Applications. *J. Mater. Chem.* **2011**, *21*, 11550–11555.
14. Wang, X.; Ren, X.; Kahen, K.; Hahn, M. A.; Rajeswaran, M.; Maccagnano-Zacher, S.; Silcox, J.; Cragg, G. E.; Efros, A. L.; Krauss, T. D. Non-Blinking Semiconductor Nanocrystals. *Nature* **2009**, *459*, 686–689.
15. Jun, Y.-W.; Choi, J.-S.; Cheon, J. Shape Control of Semiconductor and Metal Oxide Nanocrystals through Nonhydrolytic Colloidal Routes. *Angew. Chem., Int. Ed.* **2006**, *45*, 3414–3439.
16. Cozzoli, P. D.; Pellegrino, T.; Manna, L. Synthesis, Properties and Perspectives of Hybrid Nanocrystal Structures. *Chem. Soc. Rev.* **2006**, *35*, 1195–1208.
17. Park, J.; Joo, J.; Kwon, S. G.; Jang, Y.; Hyeon, T. Synthesis of Monodisperse Spherical Nanocrystals. *Angew. Chem., Int. Ed.* **2007**, *46*, 4630–4660.
18. Son, D. H.; Hughes, S. M.; Yin, Y.; Alivisatos, A. P. Cation Exchange Reactions in Ionic Nanocrystals. *Science* **2004**, *306*, 1009–1012.
19. Rivest, J. B.; Jain, P. K. Cation Exchange on the Nanoscale: An Emerging Technique for New Material Synthesis, Device Fabrication, and Chemical Sensing. *Chem. Soc. Rev.* **2013**, *42*, 89–96.
20. Pietryga, J. M.; Werder, D. J.; Williams, D. J.; Casson, J. L.; Schaller, R. D.; Klimov, V. I.; Hollingsworth, J. A. Utilizing the Lability of Lead Selenide to Produce Heterostructured Nanocrystals with Bright, Stable Infrared Emission. *J. Am. Chem. Soc.* **2008**, *130*, 4879–4885.
21. Casavola, M.; Van Huis, M. A.; Bals, S.; Lambert, K.; Hens, Z.; Vanmaekelbergh, D. Anisotropic Cation Exchange in PbSe/CdSe Core/Shell Nanocrystals of Different Geometry. *Chem. Mater.* **2012**, *24*, 294–302.
22. Grodzinska, D.; Pietra, F.; van Huis, M. A.; Vanmaekelbergh, D.; Donega, C. d. M. Thermally-Induced Atomic Reconstruction of PbSe/CdSe Core/Shell Quantum Dots into PbSe/CdSe Bi-Hemisphere Hetero-Nanocrystals. *J. Mater. Chem.* **2011**, *21*, 11556–11565.
23. Jain, P. K.; Amirav, L.; Aloni, S.; Alivisatos, A. P. Nanoheterostructure Cation Exchange: Anionic Framework Conservation. *J. Am. Chem. Soc.* **2010**, *132*, 9997–9999.
24. Sadtler, B.; Demchenko, D. O.; Zheng, H.; Hughes, S. M.; Merkle, M. G.; Dahmen, U.; Wang, L.-W.; Alivisatos, A. P. Selective Facet Reactivity during Cation Exchange in Cadmium Sulfide Nanorods. *J. Am. Chem. Soc.* **2009**, *131*, 5285–5293.
25. Miszta, K.; Dorfs, D.; Genovese, A.; Kim, M. R.; Manna, L. Cation Exchange Reactions in Colloidal Branched Nanocrystals. *ACS Nano* **2011**, *5*, 7176–7183.
26. Li, H.; Zanella, M.; Genovese, A.; Povia, M.; Falqui, A.; Giannini, C.; Manna, L. Sequential Cation Exchange in Nanocrystals: Preservation of Crystal Phase and Formation of Metastable Phases. *Nano Lett.* **2011**, *11*, 4964–4970.
27. Luther, J. M.; Zheng, H.; Sadtler, B.; Alivisatos, A. P. Synthesis of PbS Nanorods and Other Ionic Nanocrystals of Complex Morphology by Sequential Cation Exchange Reactions. *J. Am. Chem. Soc.* **2009**, *131*, 16851–16857.
28. Eilers, J.; Groeneveld, E.; Donega, C. d. M.; Meijerink, A. Optical Properties of Mn-Doped ZnTe Magic Size Nanocrystals. *J. Phys. Chem. Lett.* **2012**, *3*, 1663–1667.
29. Mocatta, D.; Cohen, G.; Schattner, J.; Millo, O.; Rabani, E.; Banin, U. Heavily Doped Semiconductor Nanocrystal Quantum Dots. *Science* **2011**, *332*, 77–81.
30. Sahu, A.; Kang, M. S.; Kompch, A.; Notthoff, C.; Wills, A. W.; Deng, D.; Winteren, M.; Frisbie, C. D.; Norris, D. J. Electronic Impurity Doping in CdSe Nanocrystals. *Nano Lett.* **2012**, *12*, 2587–2594.
31. Groeneveld, E.; van Berkum, S.; van Schooneveld, M. M.; Gloter, A.; Meeldijk, J. D.; van den Heuvel, D. J.; Gerritsen, H. C.; Donega, C. d. M. Highly Luminescent (Zn,Cd)Te-CdSe Colloidal Heteronanowires with Tunable Electron-Hole Overlap. *Nano Lett.* **2012**, *12*, 749–757.
32. Zhong, X.; Feng, Y.; Zhang, Y.; Gu, Z.; Zou, L. A Facile Route to Violet- to Orange-Emitting $Cd_xZn_{1-x}Se$ Alloy Nanocrystals *via* Cation Exchange Reaction. *Nanotechnology* **2007**, *18*, 385606.
33. Norris, D. J.; Bawendi, M. G. Measurement and Assignment of the Size-Dependent Optical Spectrum in CdSe Quantum Dots. *Phys. Rev. B* **1996**, *53*, 16338–16346.
34. Kolomiets, B. T.; Lin, C. Spectral Distribution of the Internal Photoelectric Effect in the ZnSe-CdSe System. *Sov. Phys. Solid State* **1960**, *2*, 154–156.
35. Donega, C. d. M.; Koole, R. Size Dependence of the Spontaneous Emission Rate and Absorption Cross Section of CdSe and CdTe Quantum Dots. *J. Phys. Chem. C* **2009**, *113*, 6511–6520.

36. Donega, C. d. M.; Hickey, S. G.; Wuister, S. F.; Vanmaekelbergh, D.; Meijerink, A. Single-Step Synthesis to Control the Photoluminescence Quantum Yield and Size Dispersion of CdSe Nanocrystals. *J. Phys. Chem. B* **2003**, *107*, 489–496.
37. Van Embden, J.; Mulvaney, P. Nucleation and Growth of CdSe Nanocrystals in a Binary Ligand System. *Langmuir* **2005**, *21*, 10226–10233.
38. Dean, J. A. *Lange's Handbook of Chemistry*, 15th ed.; McGraw-Hill: New York, 1999.
39. Donega, C. d. M. Formation of Nanoscale Spatially Indirect Excitons: Evolution of the Type-II Optical Character of CdTe/CdSe Heteronanocrystals. *Phys. Rev. B* **2010**, *81*, 165303.
40. He, J.; Lo, S. S.; Kim, J.; Scholes, G. D. Control of Exciton Spin Relaxation by Electron-Hole Decoupling in Type-II Nanocrystal Heterostructures. *Nano Lett.* **2008**, *8*, 4007–4013.
41. Choi, C. L.; Li, H.; Olson, A. C. K.; Jain, P. K.; Sivasankar, S.; Alivisatos, A. P. Spatially Indirect Emission in a Luminescent Nanocrystal Molecule. *Nano Lett.* **2011**, *11*, 2358–2362.
42. Koole, R.; Schapotschnikow, P.; Donega, C. d. M.; Vlugt, T. J. H.; Meijerink, A. Time-Dependent Photoluminescence Spectroscopy as a Tool to Measure the Ligand Exchange Kinetics on a Quantum Dot Surface. *ACS Nano* **2008**, *2*, 1703–1714.
43. Vlaskin, V. A.; Beaulac, R.; Gamelin, D. R. Dopant-Carrier Magnetic Exchange Coupling in Colloidal Inverted Core/Shell Semiconductor Nanocrystals. *Nano Lett.* **2009**, *9*, 4376–4382.
44. Kambhampati, P. Unraveling the Structure and Dynamics of Excitons in Semiconductor Quantum Dots. *Acc. Chem. Res.* **2011**, *44*, 1–13.
45. Hendry, E.; Koeberg, M.; Wang, F.; Zhang, H.; de Mello Donega, C.; Vanmaekelbergh, D.; Bonn, M. Direct Observation of Electron to Hole Energy Transfer in CdSe Quantum Dots. *Phys. Rev. Lett.* **2006**, *96*, 057408.
46. Wang, H.; Donega, C. d. M.; Meijerink, A.; Glasbeek, M. Ultrafast Exciton Dynamics in CdSe Quantum Dots Studied from Bleaching Recovery and Fluorescence Transients. *J. Phys. Chem. B* **2006**, *110*, 733–737.
47. Liu, H.; Owen, J. S.; Alivisatos, A. P. Mechanistic Study of Precursor Evolution in Colloidal Group II–VI Semiconductor Nanocrystal Synthesis. *J. Am. Chem. Soc.* **2007**, *129*, 305–312.
48. Reinoso, D. M.; Damiani, D. E.; Tonetto, G. M. Zinc Carboxylic Salts Used as Catalyst in the Biodiesel Synthesis by Esterification and Transesterification: Study of the Stability in the Reaction Medium. *Appl. Catal. A: Gen.* **2012**, *449*, 88–95.
49. Shaw, D. Diffusion Mechanisms in II-IV Materials. *J. Cryst. Growth* **1988**, *86*, 778–796.
50. Cadars, S.; Smith, B. J.; Epping, J. D.; Acharya, S.; Belman, N.; Golan, Y.; Chmelka, B. F. Atomic Positional *versus* Electronic Order in Semiconducting ZnSe Nanoparticles. *Phys. Rev. Lett.* **2009**, *103*, 136802.
51. Lovingood, D. D.; Achey, R.; Paravastu, A. K.; Strouse, G. F. Size- and Site-Dependent Reconstruction in CdSe QDs Evidenced by $^{77}Se\{^{1}H\}$ CP-MAS NMR Spectroscopy. *J. Am. Chem. Soc.* **2010**, *132*, 3344–3354.
52. Groeneveld, E.; Donega, C. d. M. Enhanced Exciton-Phonon Coupling in Colloidal Type-II CdTe-CdSe Heteronanocrystals. *J. Phys. Chem. C* **2012**, *116*, 16240–16250.
53. Klimov, V. I.; Ivanov, S. A.; Nanda, J.; Achermann, M.; Bezel, I.; McGuire, J. A.; Piryatinski, A. Single-Exciton Optical Gain in Semiconductor Nanocrystals. *Nature* **2007**, *447*, 441–446.
54. Zhao, Y.; Riemersma, C.; Pietra, F.; Koole, R.; Donega, C. d. M.; Meijerink, A. High Temperature Luminescence Quenching of Quantum Dots. *ACS Nano* **2012**, *6*, 9058–9067.
55. Shirasaki, Y.; Supran, G. J.; Bawendi, M. G.; Bulović, V. Emergence of Colloidal Quantum-Dot Light-Emitting Technologies. *Nat. Photonics* **2013**, *7*, 13–23.
56. Pattantyus-Abraham, A. G.; Kramer, I. J.; Barkhouse, A. R.; Wang, X.; Konstantatos, G.; Debnath, R.; Levina, L.; Raabe, I.; Nazeeruddin, M. K.; Grätzel, M.; *et al.* Depleted-Heterojunction Colloidal Quantum Dot Solar Cells. *ACS Nano* **2010**, *4*, 3374–3380.
57. Medintz, I. L.; Uyeda, H. T.; Goldman, E. R.; Mattoussi, H. Quantum Dot Bioconjugates for Imaging, Labelling and Sensing. *Nat. Mater.* **2005**, *4*, 435–446.
58. Krumer, Z.; Pera, S. J.; van Dijk-Moes, R. J. A.; Zhao, Y.; de Brouwer, A. F. P.; Groeneveld, E.; van Sark, W. G. J. H. M.; Schropp, R. E. I.; Donega, C. d. M. Tackling Self-Absorption in Luminescent Solar Concentrators with Type-II Colloidal Quantum Dots. *Sol. Energy Mater. Sol. Cells* **2013**, *111*, 57–65.
59. Dorfs, D.; Salant, A.; Popov, I.; Banin, U. ZnSe Quantum Dots within CdS Nanorods: A Seeded-Growth Type-II System. *Small* **2008**, *4*, 1319–1323.